Chemical Engineering Journal 543 (2026) 178229

Contents lists available at ScienceDirect

Chemical Engineering Journal

journal homepage: www.elsevier.com/locate/cej

Modular microgel flow reactors for automated glycan synthesis with immobilized enzymes

Kai P. Hussnaetter [a,*,1], Maria I. Pieper [b,c,1], Ulrich Thiele [d,1], Philip Palm [a], Robert Burock [e,f], René Hennig [e], Katharina Bleher [d], Andrij Pich [b,c], Matthias Franzreb [d], Erdmann Rapp [e,f], Lothar Elling [a]

[a] Laboratory for Biomaterials, Institute for Biotechnology and Helmholtz-Institute for Biomedical Engineering, RWTH Aachen University, Pauwelsstraße 20, 52074, Aachen, Germany
[b] Functional and Interactive Polymers, Institute of Technical and Macromolecular Chemistry, RWTH Aachen University, Worringerweg 2, Aachen, 52074, Germany
[c] DWI—Leibniz-Institute for Interactive Materials e.V., Forckenbeckstraße 50, Aachen, 52074, Germany
[d] Karlsruher Institute of Technology (KIT), Institute of Functional Interfaces, Hermann v. Helmholtz, Platz 1, 76344, Eggenstein-Leopoldshafen, Germany
[e] glyXera GmbH, Brenneckestrasse 20 * ZENIT, 39120, Magdeburg, Germany
[f] Max Planck Institute for Dynamics of Complex Technical System, Bioprocess Engineering, Sandtorstrasse 1, 39106, Magdeburg, Germany

ARTICLE INFO

Keywords:
Leloir-glycosyltransferases
Enzymatic glycan synthesis
Enzyme immobilization
Enzymatic membrane reactor

ABSTRACT

Glycans are biomolecules that play roles in numerous biological processes and are becoming increasingly important for applications in biomedicine, nutrition, pharmacy, and research. Their structural diversity makes glycans attractive target molecules, but also poses a challenge in their synthesis. Compared to chemical synthesis, enzymatic glycan synthesis offers various advantages: high regio- and stereoselectivity, the use of mild reaction conditions, and better ecological and economic sustainability. Automated enzymatic glycan synthesis (AEGS) is an essential development step in making defined glycan structures efficiently accessible on a larger scale.

Here, we present a modular **Mi**crogel continuous flow **R**eactor for **A**utomated and continuous **G**lycan synthesis with immobilized **E**nzymes (MiRAGE). The enzymes are immobilized in microgels, SpyT-agarose particles, or Ni^{2+}-IDA beads using different strategies. The immobilized enzymes are integrated into reactor compartments, which are supplied with substrates via a continuous reaction buffer flow. A semipermeable membrane ensures that the enzymes as well as substrates and products are retained in the module, while by-products can be selectively removed via a crossflow stream. The modular design allows several enzymatic reaction steps to be coupled, automating the synthesis of complex glycan structures.

To this end, we demonstrate the concept towards the synthesis of the human milk oligosaccharide LNFPIII, $Lewis^X$, blood group-, and Galili epitopes. In addition, we compare the different immobilization techniques and reactor strategies in terms of consistency and yield. MiRAGE represents a robust, scalable, and versatile approach that not only enables the automated synthesis of complex glycans but can also be transferred to other biocatalytic processes.

Key points:
- Immobilization of SpyCatcher-glycosyltransferases on SpyTag agarose and microgels
- Embedment of immobilized glycosyltransferases in a continuous flow bioreactor
- Enzymatic glycan synthesis with removal of by-products and retention of biocatalysts

1. Introduction

Glycans constitute the most prevalent biopolymers on earth and are found as free oligosaccharides or as essential structural and functional elements of glycoproteins, glycolipids, and proteoglycans. Their structural diversity and biological relevance make their synthesis and characterization central goals in biotechnology and life sciences. However, the inherent complexity of glycan architectures, together with the need

* Corresponding author.
E-mail address: k.hussnaetter@biotec.rwth-aachen.de (K.P. Hussnaetter).
[1] these authors contributed equally

https://doi.org/10.1016/j.cej.2026.178229
Received 28 January 2026; Received in revised form 17 April 2026; Accepted 26 May 2026
Available online 10 June 2026

for broadly applicable synthesis platforms and advanced analytical methods, continues to present considerable challenges.

A promising strategy to overcome these limitations is the use of Leloir-type glycosyltransferases (GTs, EC 2.4.). In contrast to chemical synthesis, these enzymes enable highly controlled glycosylation in a single step, providing exceptional regio- and stereoselectivity. GTs catalyze the transfer of sugar moieties from activated sugar nucleotide donors to acceptor molecules in one-step reactions. This mode of action allows the production of complex glycans [1]. The expansion of available glycosyltransferases provides an increasingly versatile foundation for advancing glycan synthesis technologies. Despite these advantages, adapting enzymatic glycan synthesis into an automated process poses challenges in instrumentation, techniques, and operational strategies.

The principles and challenges of a versatile platform for automated enzymatic glycan synthesis (AEGS) were described before [2]. In short, the basic concept of AEGS relies on repetitive or continuous reaction cycles in which enzymatic synthesis steps are carried out, and excess substrates and by-products are then removed. To enable such a process, either enzymes or the stepwise built glycan molecules must be immobilized so that they can be retained during the reaction and reused for subsequent cycles. In the case of enzymes, immobilization enables increase of stability, enzyme lifetime, and reproducibility, as well as separation and reuse [2–6]. As there is no universal preferred immobilization strategy for all enzymes, careful comparison of available techniques is essential. For glycosyltransferases, different strategies have been described [7–11]. Accordingly, two principal strategies have emerged for stepwise glycan assembly: immobilization of the growing glycans and immobilization of the enzymes.

These strategies have led to various ideas for reactor designs, of which enzyme membrane reactors (EMR) are among the most sophisticated designs. Enzymes in these systems can either remain soluble in the reaction solution or be immobilized. Immobilization avoids extensive shear stress and resulting activity loss to biocatalysts and often leads to enhanced stability [12–14]. However, in the case of direct immobilization onto the membrane matrix, continuous flow EMR systems often result in very short contact times between the substrate and the enzyme, which can limit both the turnover rate and overall yield. Therefore, EMR systems employing soluble enzymes are generally favored to date [15]. A third approach is the immobilization of enzymes onto carriers placed in the EMR, combining the advantages of immobilization and a practically homogeneous distribution of the enzymes in the whole reactor volume.

There are few examples of successful reactor systems for glycan synthesis based on these strategies. First, the CEM Liberty Blue peptide synthesizer was adapted as a basis for an automated reactor system for enzymatic glycan synthesis [16]. Temperature-responsive polymers, specifically poly(*N*-isopropylacrylamid) conjugated to glycan substrates, serve as primer acceptor molecules. The immobilized glycans are placed in the reaction compartment together with soluble glycosyltransferases, nucleotide sugar donors, and buffer compounds. At ambient temperatures, the polymers remain soluble, allowing enzymatic glycosylation under mild conditions. Subsequent heating triggers polymer precipitation, facilitating facile separation of the polymer-bound glycans from the reaction mixture. Denatured enzymes, unreacted nucleotides, and buffer components are removed through washing and filtration, while the precipitated glycans are retained. For the next cycle, cooling re-solubilizes the polymer, enabling the addition of fresh nucleotide sugars, enzymes, and buffer to continue the next glycosylation cycles. As a demonstration, GM1 ganglioside was synthesized from lactose through three sequential enzymatic steps, yielding 38% substrate conversion in 15 h [16].

In the second example, synthesis of soluble glycans was achieved using immobilized enzymes within a compartmented microfluidic flow reactor system [17,18]. In this setup, different glycosyltransferases were immobilized on magnetic beads suspended in different aqueous droplets with ethyl acetate as a separation fluid. While fixing the magnetic beads by an external magnetic field, the droplets with dissolved sequentially growing glycans could be transferred from one enzyme carrier to the next, initiating the next synthesis step. Compartmentation enabled stable enzyme localization while allowing donor substrate and intermediate glycans to be efficiently shuttled to subsequent modules. For the example of non-sulfated HNK-1 synthesis, the system achieved 96% yield after only 210 min for two GT steps. This shows that combining compatible enzymatic reactions in various configurations under optimal conditions makes it possible to construct effective enzyme cascades; however, the microfluidic droplet approach is difficult to scale up. Therefore, we focus on the third strategy, the combination of enzyme immobilization in particulate carriers with scalable membrane reactors.

An important precondition of this strategy for the automation of enzymatic glycan synthesis is the immobilization of GTs in suitable carriers. While enzyme immobilization has been demonstrated using a variety of support materials like metal-organic frameworks (MOFs) [19], covalent organic frameworks (COVs) [20] or hydrogels [21], microgels offer several advantages as enzyme carriers, including lower internal mass-transfer limitations (like in hydrogels [21]) and a water-rich microenvironment without rigid confinement (like in MOFs and COVs that otherwise require careful tuning [19,20,22]). In addition, the chemistry used for microgel fabrication can be precisely tuned to optimize enzyme stability and activity [23], and they exhibit good hydrodynamic behavior for instance in membrane-retained slurries [24]. Previously, Sommerfeld, Palm and Hussnaetter [7] presented a droplet-based microfluidic approach for the production of microgels with immobilized GTs through encapsulation or post-attachment. They confirmed enzyme immobilization and demonstrated that the immobilized enzymes retain their catalytic activity for GT-mediated glycan synthesis. Palm et al. [8] focused more specifically on the immobilization of glycosyltransferases onto SpyTag-functionalized agarose via SpyTag-SpyCatcher coupling. After enzyme coupling, the immobilized enzymes retain substantial activity, exhibit improved long-term stability, and allow repeated reuse over multiple reaction cycles [2,7,8].

The other precondition of automated enzymatic glycan synthesis is the development of suitable reactor concepts. The respective implementation of a modular immobilized enzyme membrane reactor (IEMR) poses several design challenges. First, a suitable retention membrane has to be selected that will enable selective permeation: enzymes, substrates, and target products should be retained in the reactor, while by-products and buffer components should be able to pass freely. In general, the separation behavior in the IEMR depends on the selected membrane molecular-weight cut-off (MWCO), which can be adapted to the specific application. Low-molecular-weight side products may permeate the membrane, whereas larger glycans are retained. As a practical rule of thumb, effective separation is facilitated when the retained species has a molecular weight of approximately three times that of the permeating component. In addition, for the in-situ removal of unwanted side products the same reactor modules should be able to operate in an effective crossflow mode, removing the contaminants while keeping the intermediate or end products [13,14,25]. In the present study, the primary aim was not to establish a fully optimized preparative production process, but to demonstrate the proof-of-concept of a modular flow platform for automated glycan synthesis with immobilized enzymes. In particular, the reactor was designed to enable both sequential packed-bed type reactions and buffer exchange between enzymatic steps, which is essential for multistep syntheses requiring changing reaction conditions. In addition, crossflow operation was investigated as an integrated process-conditioning strategy to remove low-molecular-weight side components during synthesis rather than as a standalone final purification step. Against this background, the present study establishes and evaluates a modular immobilized-enzyme membrane reactor (IEMR) as a proof-of-concept platform for automated multistep glycan synthesis, with particular emphasis on combining sequential packed-bed type reactions with buffer exchange and crossflow-assisted in situ removal of low-molecular-weight side components. As a demonstration

of applicability, the platform was applied to the synthesis of biologically relevant glycans including LNFPIII, the Galili epitope, blood group A epitope, and Lewis^X.

2. Material and methods

2.1. Materials

HPLC-grade water for droplet-based microfluidic synthesis and preparation of buffers, *N*-(2-Hydroxyethyl)piperazine-*N*′-(2-ethanesulfonic acid) (HEPES, 99%), sodium hydroxide (99.5%), KCl (85%), and the Sylgard 184 elastomer kit were purchased from Merck (Sigma-Aldrich) and used as received. *n*-heptane (99.9%) was purchased from VWR (Avantor, Radnor, PA, USA). Aquapel was purchased from PGW Auto Glass, LLC (Cranberry, PA, USA). The surfactant FluoSurf™ and the hydrofluoroether (HFE-7500) oil were purchased from Emulseo (Pessac, France). Methacryloxyethyl thiocarbamoyl rhodamine B (RB) (98%) was purchased from Polysciences Inc. (Warrington, PA, USA). All poly (ethylene glycol) (PEG) with vinylsulfone functionalization (PEG-VS) were purchased from CreativePEGWorks (Chapel Hill, NC, USA). PEGs with thiol functionalization (PEG-SH) were purchased from Biopharma PEG Scientific Inc. (Watertown, MA, USA). PureCube Maleimide Activated Agarose was purchased from Cube Biotech (Monheim am Rhein, Germany). The SpyTag (CRGVPHIVMVDAYKRYK, 2034.06 g mol^{-1}, 98%) was purchased from BioCat (Heidelberg, Germany).

2.2. Glycosyltransferase plasmid construction

Plasmids for protein production in *Escherichia coli* were designed with a similar plasmid architecture, allowing a cassette system-based exchange of different genetic elements with a pETDuet-1 vector as backbone. Each SpyCatcher-glycosyltransferase (SpyC-GT) construct begins with a His_6-tag and the SpyCatcher003 domain from *Streptococcus pyogenes* [26], which serves as an immobilization tag positioned at the N-terminus of the fusion protein. This domain is connected via a short, flexible glycine–serine linker [27] to a solubility tag. As solubility tags, either the lipase pro-peptide (LPP) from *Staphylococcus hyicus* [28] or the maltose-binding protein (malE, MBP) from *E. coli* K-12 [29] were employed. After an additional glycine-serine linker, the respective glycosyltransferase (GT) was fused at the C-terminus. Importantly, the architecture of the plasmid SpyC-α3,4FucT slightly differs, since the glycosyltransferase of the translated protein is located at the N-terminus of the fusion protein. Noteworthy, this bifunctional enzyme exhibits both, α1,3 and α1,4 FucT activity depending of the acceptor substrate (LacNAc type 2 or LacNAc type 1). While this feature offers a broader possibility of application, for the synthesis of target glycans Lewis^X and LNFPIII from LacNAc type 2 and LNnT, respectively, only the α1,3 activity was relevant [30].

All constructs were designed using CloneManager 9.0 (Sci Ed Software, Westminster, CO, USA) and synthesized and purchased from BioCat (Heidelberg, Germany). Detailed plasmid design was described before, including SpyC-β4GalT, SpyC-α3GalT, SpyC-α3GlcNAcT (SpyC-LgtA) [7], SpyC-α3GalNAcT (SpyC-GTA) [8,31], and α2FucT (FutC) [30,32]. A list of all utilized enzymes is depicted in Table 1 and Table S3.

2.3. Production of glycosyltransferases

Expression plasmids were introduced into different chemically competent *E. coli* expression strains by heat-shock transformation according to the manufacturer's protocol. Specifically, SpyC-α3,4FucT, FutC, and SpyC-GTA were transformed into BL21 (DE3) (NEB, Ipswich, MA, USA), SpyC-LgtA into Rosetta 2 (DE3) pLysS (Merck, Darmstadt, Germany), and SpyC-β4GalT into SHuffle T7 Express (NEB, Ipswich, MA, USA) (Table 1). Cultivation and heterologous expression were performed as previously described [8,33]. Briefly, transformed *E. coli* were pre-cultivated overnight in 20 mL LB medium and subsequently transferred to 1 L TB medium in 5 L baffled flasks, grown at 37 °C and 80 rpm. At an OD_{600} of 0.5–0.8, expression was induced with 0.1 mM isopropyl-β-D-thiogalactopyranoside (IPTG), and cultivation continued at 25 °C for 20–24 h. Cells were harvested by centrifugation, and pellets were stored at −20 °C until further use. For purification via immobilized metal ion affinity chromatography (IMAC), 4 g of the cell pellet were resuspended in 10 mL lysis/binding buffer (20 mM imidazole, 250 U Pierce Nuclease, Table 1) and lysed by sonication. After centrifugation, the supernatant was filtered (0.8 µM, low protein binding) and loaded onto a HisTrap HP Ni^{2+}-NTA column for His_6-tag affinity purification on an ÄKTA system (Cytiva, Marlborough, MA, USA). Non-specifically bound proteins were washed off with lysis/binding buffer (20 mM imidazole, Table 1), following elution of immobilized target protein by elution buffer (500 mM imidazole, Table 1). Enzymes were dialyzed overnight against the respective storage buffer (Table 2). Concentration, identity, and integrity were confirmed by Bradford assay, SDS-PAGE, Western blot analysis, and activity assay.

2.4. Glycosyltransferase activity assays

To verify enzyme activity and define reaction parameters, activity assays were performed for free enzymes, SpyT-agarose-immobilized enzymes, and microgel-immobilized enzymes. Respective *t*Boc-linked glycan acceptors (5 mM) and nucleotide sugar donors (6.5 mM) were mixed with the specific (immobilized) glycosyltransferases in a defined buffer system. The reaction was incubated at 30 °C, and samples were

Table 1
Origin, expression host, and purification buffer of the used glycosyltransferases.

Enzyme name	Enzyme type	Origin organism	*E. coli* expression strain	IMAC buffer
SpyC-β4GalT	β1,4-galactosyltransferase 1	*Homo sapiens*	SHuffle T7 Express	20 mM Na_2HPO_4, 500 mM NaCl, pH 7.4
SpyC-α3GalT	α1,3-galactosyltransferase	*Mus musculus*	BL21 (DE3)	50 mM HEPES; 500 mM NaCl pH 7.5
SpyC-LgtA	β1,3-*N*-acetylglucosaminyltransferase	*Neisseria meningitidis*	Rosetta 2 (DE3) pLysS	50 mM TRIS-HCl, 500 mM NaCl, pH 7.5
FutC	α1,2- fucosyltransferase	*Helicobacter pylori*	BL21 (DE3)	50 mM TRIS-HCl, 500 mM NaCl, pH 7.5
SpyC-GTA	α1,3-*N*-acetylgalactosaminyltransferase	*Homo sapiens*	BL21 (DE3)	50 mM TRIS-HCl, 500 mM NaCl, pH 7.5
SpyC-α3,4FucT	α3,4- fucosyltransferase	*Helicobacter pylori*	BL31 (DE3)	50 mM TRIS-HCl, 500 mM NaCl, pH 7.5

Table 2
Storage buffer, substrates, and reaction buffer of the used glycosyltransferases.

Enzyme name	Enzyme type	Storage buffer	Substrates[a]	Reaction buffer
SpyC-β4GalT	β1,4-galactosyltransferase 1	100 mM glycine, pH 10	GlcNAc-*t*Boc UDP-Gal	100 mM Glycine pH 10, 5 mM $MnCl_2$ 20 U mL^{-1} FastAP
SpyC-α3GalT	α1,3-galactosyltransferase	100 mM HEPES 500 mM KCl, pH 7.5,	LacNAc-*t*Boc UDP-Gal	100 mM HEPES pH 7, 150 mM KCl, 2 mM $MnCl_2$, 1% glycerol, 1 mg mL^{-1} BSA 20 U mL^{-1} U FastAP
SpyC-LgtA	β1,3-*N*-acetylglucosaminyltransferase	100 mM glycine, pH 10	lactosyl-*t*Boc UDP-GlcNAc	100 mM Glycine pH 10, 5 mM $MnCl_2$, 20 U mL^{-1} FastAP
FutC	α1,2- fucosyltransferase	50 mM TRIS-HCl, 100 mM NaCl, pH 7.5	lactosyl-*t*Boc GDP-Fuc	100 mM TRIS-HCl pH 6, 25 mM KCl, 5 mM $MnCl_2$, 5 mM $MgCl_2$, 20 U mL^{-1} FastAP
SpyC-GTA	α1,3-*N*-acetylgalactosaminyltransferase	50 mM TRIS-HCl, 100 mM NaCl, pH 7.5	2′-FL (2′-fucosyl lactose)-*t*Boc UDP-GalNAc	100 mM MOPS pH 7, 20 mM $MgCl_2$, 1 mg mL^{-1} BSA 20 U mL^{-1} FastAP,
SpyC-α3,4FucT	α3,4- fucosyltransferase	50 mM TRIS-HCl, 100 mM NaCl, pH 7.5	LacNAc-*t*Boc GDP-Fuc	100 mM HEPES 25 mM KCl 2 mM $MnCl_2$ 20 U mL^{-1} FastAP

[a] Substrates for the initial activity assay are shown. Acceptor molecules might differ for cascades and are described in the respective reactor module (Table 4).

taken at defined time points, denatured at 95 °C to stop enzyme activity, and centrifuged. The supernatant was analyzed via high-performance liquid chromatography with UV detection (HPLC-UV).

2.5. Immobilization of glycosyltransferases

2.5.1. Immobilization in microgels

Microgels were prepared in a droplet-based microfluidic device prior to or parallel to immobilization of glycosyltransferases. Microgels were characterized by nanoindentation measurements, micropipette aspiration, confocal laser scanning microscopy and fluorescence recovery after photo bleaching.

2.5.1.1. Fabrication of droplet-based microfluidic devices. A master mold template with two inlets for a dispersed phase, one inlet for a continuous phase, and one outlet was designed with the AutoCAD software (Autodesk, San Rafael, CA, USA). The design was printed on a dark-field photomask at 25,000 dpi with a channel width of 80 µm. Soft lithography was used to transfer the design onto an SU-8 epoxy-based photoresist attached to a silicon wafer. A 10:1 mixture of poly(dimethylsiloxane) (PDMS) and curing agent Silgard 184 elastomer kit (Dow Corning, Midland, MI, USA) was degassed and poured into this master mold [34], which was cured at 60 °C overnight. The device was carefully removed from the master mold using a scalpel. The inlets and outlets were punched with a biopsy puncher (MicrotoNano, diameter: 0.75 mm, Haarlem, Netherlands). After the device as well as a glass slide were cleaned in 2-propanol in an ultrasonic bath for 10 min, both parts were washed at least three times with 2-propanol and distilled water each. The device and glass slide were dried in an oven overnight and bonded after oxygen plasma treatment (30 mL min^{-1}, 100 W, 40 s). Lastly, the channels were flushed with Aquapel and then air to make the channels hydrophobic and remove excess Aquapel, respectively.

2.5.1.2. Synthesis of microgels. Two different aqueous or dispersed phases were used for the production of microgels, one containing PEG functionalized with thiols (SH phase) and one containing PEG functionalized with vinylsulfone groups (VS phase). Eight different methods were tested for the immobilization of enzymes in microgels [7]: the enzymes could either be encapsulated during the synthesis of the microgels with covalent attachment (cov) or through non-covalent encapsulation (noncov), or the enzymes could be incorporated after the synthesis in a post-attachment step by covalent attachment onto vinylsulfone groups (VS) or through SpyTag-SpyCatcher interaction (SpyT). For the covalent attachment, thiol groups in the enzymes can undergo Michael-type addition reactions with free vinylsulfone groups of the PEG stars during the gelation of the droplets. In the non-covalent approach, no free vinylsulfone groups are present, so the enzymes are only sterically entrapped inside the network through the formation of the microgel network around them. For both post-attachment methods, free reactive groups, either vinylsulfone groups (VS) or SpyTags (SpyT) that were incorporated into the microgel during the microfluidic reaction, are present after purification and can then undergo Michael-type addition with thiols or SpyTag-SpyCatcher interactions with SpyCatcher moieties of the enzymes, respectively. This also yields covalent bonds for efficient enzyme immobilization.

All of these were tested for larger molecular weight PEGs (−L) and smaller molecular weight PEGs (-S). The masses of the chemicals used for the synthesis can be found in Table 3. For the VS phase, PEG-VS was

Table 3
Composition of the VS phase and SH phase used for the eight different enzyme immobilization methods.

Method	VS phase	SH phase	Enzyme/ SpyTag
cov-L	30 mg 8-arm-PEG-VS 20 kDa	15 mg 4-arm-PEG-SH 10 kDa	Enzyme
cov-S	30 mg 8-arm-PEG-VS 10 kDa	15 mg 4-arm-PEG-SH 5 kDa	Enzyme
noncov-L	15 mg 4-arm-PEG-VS 10 kDa	15 mg 4-arm-PEG-SH 10 kDa	Enzyme
noncov-S	15 mg 4-arm-PEG-VS 5 kDa	15 mg 4-arm-PEG-SH 5 kDa	Enzyme
VS-L	30 mg 8-arm-PEG-VS 20 kDa	15 mg 4-arm-PEG-SH 10 kDa	–
VS-S	30 mg 8-arm-PEG-VS 10 kDa	15 mg 4-arm-PEG-SH 5 kDa	–
SpyT-L	30 mg 8-arm-PEG-VS 20 kDa	15 mg 4-arm-PEG-SH 10 kDa	SpyTag
SpyT-S	30 mg 8-arm-PEG-VS 10 kDa	15 mg 4-arm-PEG-SH 5 kDa	SpyTag

dissolved in 300 µL 100 mM HEPES pH 8 buffer. For the SH phase, PEG-SH was dissolved in 150 µL 100 mM HEPES pH 8 buffer, or HPLC-grade water in the case of SpyT-L and SpyT-S microgels. To this, 0.7 µL of a 4.5 *w/v*% methacryloxyethyl thiocarbamoyl rhodamine B (RB) solution was added and shaken thoroughly. Lastly, 149.3 µL of an enzyme solution in buffer or a 2 w/v% SpyTag solution in water were added, and the mixture was shaken again.

The solutions, as well as an oil phase consisting of fluorocarbon oil (HFE-7500) with 2 wt% FluoSurf™ surfactant (Emulseo, Pessac, France), were transferred to three separate syringes (1000 series, Gastight, with luer tip; Hamilton, Bonaduz, Switzerland). The syringes were mounted on syringe pumps (PHD Ultra, Harvard Apparatus, Holliston, MA, USA) and connected to the microfluidic device via fine-bore polyethylene tubing (inner diameter: 0.40 mm, outer diameter: 1.10 mm). The flow rates were adjusted to 150 µL h^{-1} for each aqueous phase and to 600 µL h^{-1} for the oil phase. The synthesis was observed with an inverted microscope (Motic AE2000, TED PELLA Inc., Redding, CA, USA) and recorded with an attached camera (Flea3, Point Gray, Richmond, CA, USA). The emulsion was collected and left to react in a fridge overnight. For the purification of the microgels, the supernatant was exchanged three times against HFE-7500 oil, once against n-heptane, and at least three times against HEPES pH 7 buffer with 150 mM KCl. In between purification steps with buffer, the microgels were centrifuged at 8000 rpm for 15 s to accelerate the sedimentation of the microgels.

For enzyme immobilization techniques through post-attachment (VS and SpyT), 200 µL of concentrated microgel dispersion, 1 mL HEPES pH 7 buffer, and 200 µL enzyme solution were mixed and shaken for 24 h at room temperature at 500 rpm. During purification, the first supernatant was collected to determine the non-immobilized enzyme content through a Bradford assay. The purification was performed by exchanging the solvent with fresh buffer at least three times.

2.5.1.3. Nanoindentation. Nanoindentation measurements were performed on a high-throughput mechanical screening Nanoindenter Pavone (Optics11Life, Amsterdam, The Netherlands). For each microgel, a minimum of 50 indentations were performed. Microgels were attached to a well plate by drying and rehydrating with water at room temperature. All measurements were performed using a cantilever-based probe with a spherical tip (8 µm radius, 0.45 N m^{-1} stiffness) in peak load poking mode, aiming for a maximum indentation depth of 16% of the tip radii. The Hertzian model was used to determine the effective Young's modulus E_{eff} by fitting the load-indentation curves [35].

2.5.1.4. Micropipette aspiration (MPA). For micropipette aspiration measurements, micropipettes were pulled from borosilicate glass capillaries with an outer diameter of 1.50 mm and an inner diameter of 1.17 mm using the p-1000 micropipette puller from Sutter Instruments (Novato, CA, USA). The pulled capillaries were cut with a heating wire attached to a MicroData Instruments Inc. (South Plainfield, NJ, USA) microscope for visualization during cutting. The micropipette was connected to the PatchServer Main Unit (Multichannel Systems, Reutlingen, Germany) via an Axopatch holder with a suction port and wire (A-M Systems, Maulbronn, Germany). The PatchServer and PatchMaster software were used to control the applied negative pressure during the measurements. Microscopy images of the aspirated microgels were taken using a Leica DMi8 microscope and the LAS X software.

The images of the aspirated microgels were analyzed regarding the pipette radius R_p and the aspirated length Δx with the software ImageJ. For each sample, at least 3 microgels were investigated at 10 different applied negative pressures. The applied force F was calculated using the applied negative pressure and the diameter of the capillary orifice, and plotted against the normalized aspirated length of the microgel. The resulting graphs were fitted with a linear fit. The obtained slope s was used to determine the Young's modulus E using eq. (1) with a continuum-medium model (eq. (2)). This model assumes homogeneity and ϕ_p is assumed to be 2.1 [36].

$$\frac{\Delta P}{E} = \frac{2\pi\Delta x}{3\phi_p R_p} \tag{1}$$

$$E = s\frac{3\phi_p}{2\pi^2 R_p} \tag{2}$$

2.5.1.5. Confocal laser scanning microscopy (CLSM). For confocal laser scanning microscopy (CLSM), a Leica TCS SP8 confocal microscope (Leica, Wetzlar, Germany) was used. Brightfield images were taken with a PMT trans detector. RB was excited with a DPSS laser at a wavelength of 561 nm and detected with a HyD detector between 575 and 620 nm. For the fluorescamine assay, 40 µL of a microgel dispersion were transferred onto a glass slide before adding 10 µL of a 3 mg mL^{-1} solution of 4′-phenylspiro[2-benzofuran-3,2′-furan]-1,3′-dione (fluorescamine) in acetone and quickly mixing. The fluorophore was excited at 390 nm with an argon laser and detected between 450 and 500 nm using a HyD detector. Images were taken with the LAS X software.

2.5.1.6. Fluorescence recovery after Photobleaching (FRAP). For FRAP measurements [37], 10 µL of a concentrated microgel dispersion were added to 100 µL of a 1 mg mL^{-1} 4 kDa FITC-dextran solution in water. FRAP measurements were performed on the CLSM setup as described above. The FITC-dextran was excited with an argon laser at a wavelength of 488 nm, and the fluorescence was detected between 500 and 550 nm using a PMT detector. A spherical region of interest (ROI) in the middle of the microgels with a diameter of 40 µm was bleached with the argon laser at 488 nm and 100% laser power. For the pre-bleach, 20 images were taken 96 ms apart. During bleaching, 20 images were taken 96 ms apart. After bleaching or during fluorescence recovery, 80 images were taken at 96 ms intervals, and 30 images were taken at 1 s intervals. Using LAS X, three ROIs were applied to the images of the microgels to determine the change in fluorescence in three regions: The ROI used for the bleaching, a square covering the complete image, and one covering the background. With these ROIs, a background correction and normalization of the fluorescence intensity were performed in Origin. The normalized fluorescence recovery curves were plotted and fitted with the Soumpasis fit. In this case, the fit function was extended by the term F_0 to consider that the fluorescence at $t = 0$ was not set to 0. The equation used for the Soumpasis fit [38,39] of the recovery function $F(t)$ can be found below (eq. (3)). k is the fraction of mobile species, t is the time, τ_D is the characteristic diffusion time, and I_0 and I_1 are the zero- and first-order modified Bessel functions, respectively.

$$F(t) = k \bullet e^{-\frac{\tau_D}{2t}}\left[I_0\left(\frac{\tau_D}{2t}\right) + I_1\left(\frac{\tau_D}{2t}\right)\right] + F_0 \tag{3}$$

After fitting, the diffusion coefficient D was calculated using eq. (4) after the radius of the bleach point w was determined from the full width at half maximum from the intensity profile in LAS X.

$$D = \frac{w^2}{\tau_D} \tag{4}$$

2.5.2. Immobilization on maleimide-activated agarose via SpyC-SpyT interaction

Immobilization of SpyC-glycosyltransferases to SpyTag-maleimide-activated agarose was described before [8]. In short: for the coupling of SpyT to agarose, a modified SpyT (peptide sequence: `CGSGRGVPHIVMVDAYKRYK`) and the maleimide-activated agarose (Cube Biotech, Monheim am Rhein, Germany) were equilibrated in coupling buffer (100 mM sodium acetate, 150 mM NaCl, pH 6.5). In the following, SpyT was added to the agarose with a concentration of 5 mg·mL^{-1} agarose and subsequently incubated at room temperature overnight in an end-over-end shaker. The coupling reaction was halted by three washing and centrifugation steps, and the SpyT-agarose was stored as a

1:1 agarose/buffer suspension in coupling buffer at 4 °C. For the coupling of SpyC-GTs with SpyT-agarose via SpyC-SpyT interactions [40], the SpyT-agarose was equilibrated in the respective SpyC-GT storage buffer (Table 2). 1.5 mg of enzyme was added to 1 mL equilibrated SpyT-agarose, and the mixture was incubated at 4 °C overnight in an end-over-end shaker. The coupling reaction was again halted by several washing and centrifugation steps. The wash fractions were analyzed to verify the coupling of SpyT and the SpyC-GTS, and the enzymatic activity of immobilized SpyC-GTs was proven by an activity assay as stated above. SpyT-agarose immobilized SpyC-GTs were stored as a 1:1 SpyT-agarose/buffer suspension in the respective storage buffer (Table 2) at 4 °C.

2.5.3. *Immobilization on Ni^{2+}-IDA beads*

Immobilization of His_6-tagged glycosyltransferases to IDA-Ni functionalized magnetic beads (Cube Biotech, Monheim am Rhein, Germany) was conducted according to the manufacturer's protocol and was described before [18]. In short: 200 µL beads were washed 3 times with (100 mM TRIS, 150 mM KCl, pH 7.4) and were incubated with 2 mg respective enzyme for 3 h at 24 °C, continuously shaking. After incubation, the beads with immobilized enzymes were washed 3 times again, and wash fractions were analyzed to verify efficient binding.

2.6. *3D-printed enzymatic membrane reactor*

Continuous enzymatic glycan synthesis was performed with different setups assembled from multiple modules of a 3D-printed immobilized enzyme membrane reactor (IEMR), whose design is based on a previously introduced single-pass diafiltration module [41]. The manufacturing was conducted via 3D-printing with a PolyJet Objet260 Connex3 (Stratasys, Eden Prairie, USA) using VeroClear material. After the printing process, support material was manually removed from the surface, and internal channels were cleared by immersing the reactor parts into a 2 M NaOH solution for 24 to 48 h, followed by rinsing with water.

The IEMR mainly consists of three individually printed parts: a middle compartment and two identical lateral compartments (Fig. 1A). The middle compartment, through which the reaction mixture passes and which is filled with microgel-immobilized enzymes, is enclosed by two rectangular nanofiltration membrane sheets, which are fixed between the middle and the lateral compartments. The assembled module is held together by ten 40 mm M3 screws. A schematic visualization of the reactor reaction setup is given in Fig. 1B.

Three distinct operating modes can be realized with the identical IEMR module, corresponding to (i) reaction mode, (ii) diafiltration mode, and (iii) combined reaction/diafiltration mode (cf. flow schemes in Fig. 2). In reaction mode, the reaction mixture is passed solely through the central compartment, which is packed with microgel-immobilized enzymes, while no crossflow is applied in the lateral buffer compartments. This operating mode was used in all syntheses described in this work, either for the entire course of the reaction or as an initial phase until a sufficient amount of by-products had accumulated to warrant activation of the combined reaction/diafiltration mode. In pure diafiltration mode, the central compartment is used merely as a hold-up volume without immobilized enzyme, while a buffer solution is passed in crossflow via the lateral compartments, generating a transmembrane flux for selective removal of small solutes. This configuration has been investigated in detail in a recent study by Thiele et al. [42], in

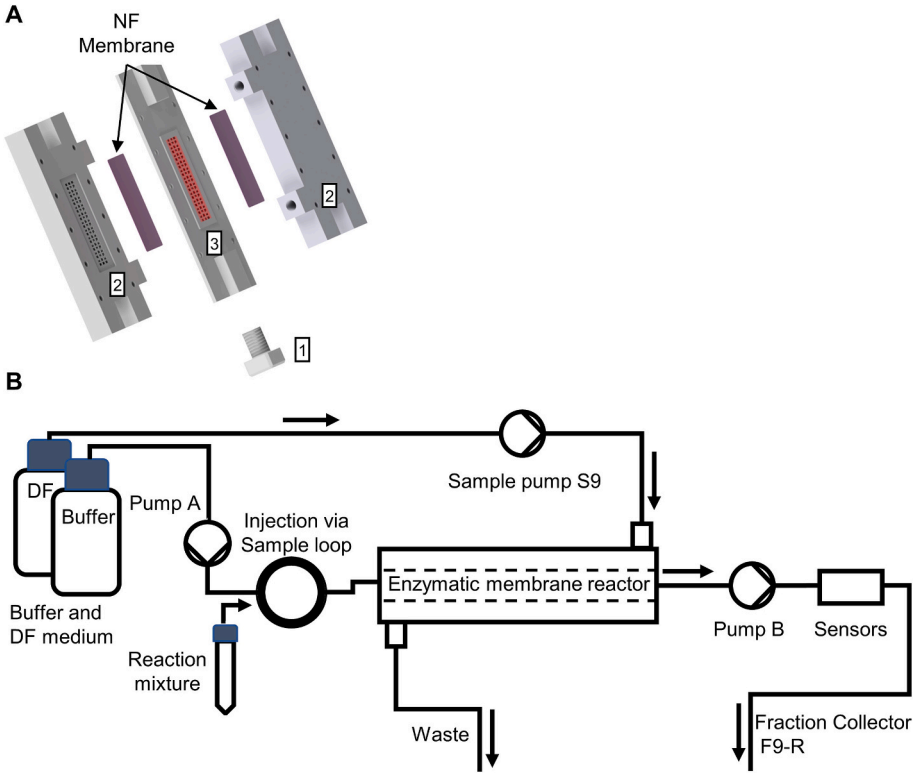

Fig. 1. Design of the 3D-printed enzymatic membrane reactor module and process scheme. (A) Assembly of module parts – 1: 3D-printed adapter for FPLC capillaries; 2: identical lateral parts with connectors for diafiltration (DF) medium inlet and permeate outlet. In each lateral part, one of the connectors is closed with a blind plug so that the diafiltration medium must flow through the membranes via the middle compartment.; 3: middle compartment with hollow-carved grid structure used for membrane support and as flow distributor in the reaction chamber (in red). (B) Process scheme illustrating the operation mode with flow through enzymatic reaction in the central compartment combined with a crossflow of DF medium for simultaneous removal of unwanted side-products (cf. Fig. 2C). The different flows of the setup are controlled by an ÄKTA plus 25 system using pump A and B for adjusting the in- and outflow of the central compartment and the independent sample pump for adjusting the flow of the DF medium. After initial flushing of the central compartment with plain buffer, the synthesis is started by switching the flow path of pump A in a way that the reaction mixture stored in a 5 mL sample loop is pumped into the reactor module.

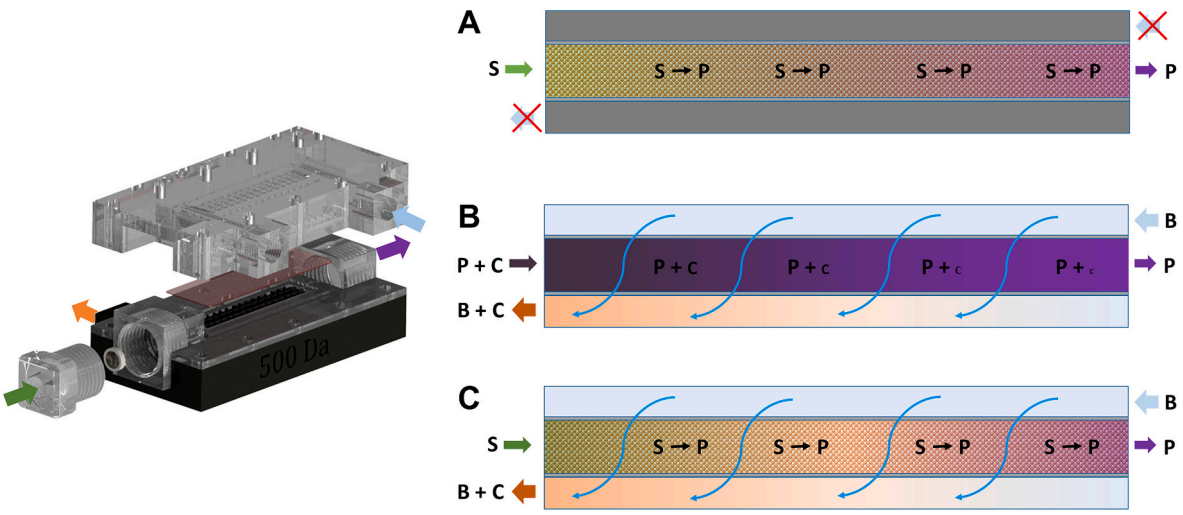

Fig. 2. Sketch and possible operations modes of the developed immobilized enzyme membrane reactor (IEMR) modules. Left: Rendered drawing with arrows indicating various in- and outlet streams. Green – substrate feed, Purple – product effluent, Blue – Buffer inlet, Orange – effluent of spend buffer and contaminants. Right: (A): Operation as flow through enzyme reactor without crossflow, (B): Operation as plain double membrane crossflow module, (C): Operation as enzyme reactor with combined in situ removal of contaminating by-products.

which the diafiltration mode was experimentally validated with various oligosaccharide nucleoside mixtures. In the context of enzymatic reactions that are not directly inhibited or otherwise disturbed by by-products, a sequential arrangement of a pure reaction module (reaction mode) followed by a pure diafiltration module (diafiltration mode) is advantageous. Such a configuration minimizes the risk of substrate loss into the permeate and reduces unfavorable concentration polarization of the substrate in the central compartment. However, it also entails longer overall residence times and a more complex synthesis setup. In the combined reaction/diafiltration mode, immobilized enzymes are retained in the central compartment while the reaction mixture is supplied through this compartment and, at the same time, an independent diafiltration stream is delivered through one lateral compartment and permeate is withdrawn through the other one. By this a crossflow across both nanofiltration membranes is generated while the enzymatic reaction takes place. This operation enables in situ removal of low-molecular-weight by-products while the enzymatic conversion proceeds, and it allows gradual adjustment of the pH and ionic composition of the reaction medium during the synthesis. In conventional crossflow filtration, membrane-permeable side products are removed with the permeate, whereas retained compounds accumulate in the retentate, thereby increasing the relative purity of the retained product. In the present double-membrane reactor, the associated volume loss is compensated by simultaneous inflow of fresh buffer through the opposite membrane. This allows low-molecular-weight side products to be depleted to the desired extent without excessive concentration of retained glycans or other retained solutes. To keep the proof-of-concept syntheses presented here technically simple while still exploiting the potential of the system, we employed an initial reaction phase in pure reaction mode, followed by a second phase in the combined reaction/diafiltration mode within the same IEMR module. Finally, a closer look at the lateral compartments in Fig. 1A reveals two tube connectors at each compartment. In future studies this will allow an alternating flow direction of the diafiltration medium as described and experimentally realized by Tan et al. [41].

2.7. General procedure for enzymatic glycan synthesis in enzymatic membrane reactor modules

Continuous glycan synthesis experiments were performed with an automated ÄKTA pure 25 FPLC setup (Cytiva, Global Life Sciences Solutions USA LLC, Marlborough, MA, USA) and 3D printed IEMR modules described above. Microgel-immobilized enzymes were added to the middle compartment, and the reactor was closed by clamping the lateral compartments with the screws. A Synder Filtration™ flat-sheet nanofiltration membrane purchased from Sterlitech Corporation (Auburn, WA, USA) was positioned between the middle and lateral compartments of the module. The assembled reactor module was installed on top of the column valve of the ÄKTA system, simplifying the removal of air from the module as well as the system.

Initially the IEMR was equilibrated at a flow rate of 10 µL min^{-1} with equilibration buffer (100 mM TRIS, 150 mM KCl, pH 7.4) prior to switching the feed to the reaction mixture (100 mM TRIS, 25 mM KCl, pH 7.4) stored in a 5 mL sample loop. A summary of the different reaction buffers, substrates, and enzyme carriers applied in the multiple reaction sequences tested is given in Table 4. In addition, 20 U mL^{-1} thermosensitive alkaline phosphatase FastAP (ThermoFisher Scientific, Waltham, MA, USA) was added to the reaction mixture in order to digest the nucleotide by-products. If applied, the diafiltration stream (100 mM Tris, 150 mM KCl, pH 7.4) was injected through the sample pump after 200 min at a flow rate of 40 µL min^{-1}. Samples were collected in 20 min fractions with an ÄKTA Fraction Collector F9-R (Cytiva, Global Life Sciences Solutions USA LLC, Marlborough, MA, USA) and analyzed via capillary electrophoresis with UV detection (CE-UV) for nucleosides and nucleotide sugars and high-performance liquid chromatography with UV detection (HPLC-UV) for *t*Boc-linked glycans or multiplexed capillary gel electrophoresis with laser-induced fluorescence detection (xCGE-LIF) for APTS labeled glycans.

Modes of reaction operation, utilized enzymes and immobilization techniques, buffer composition and substrates as well as synthesized products are described in Table 4.

2.8. Analysis of glycans and by-products

Separation and detection of *t*Boc-linked glycans was performed by HPLC-UV analysis at a wavelength of 254 nm. Glycans without modification were labeled with 8-aminopyrene-1,3,6-trisulfonic acid (APTS) and analyzed by multiplexed capillary gel electrophoresis with laser-induced fluorescence detection (xCGE-LIF). Nucleosides, nucleotides, and nucleotide sugars were measured using a capillary electrophoresis device with UV detection (CE-UV) at an adsorption wavelength of 254 nm. For calculation of concentrations, respective calibration curves are given in Fig. S7. A detailed explanation on calculation of the *t*Boc glycan standard is given in Fig. S8 and Table S8.

Table 4
Overview of reactor glycan synthesis reactions. For each reaction, composition of the 5 mL reaction buffer, substrates, immobilization method and glycan product are shown. For reaction sequences, see Fig. 3. Immobilization techniques are listed in Table S3. Descriptions of used nucleotide sugars and used and produced glycans are listed in Table S1 and Table S2.

Enzyme	Immobilization technique	Nucleotide sugar	Acceptor glycan	Product
Reaction (i) Lacto-*N*-fucopentaose III				
Approach: Transfer of intermediate reaction mix from previous to following reactor modules				
Buffer composition:		100 mM TRIS-HCl pH 7.5, 25 mM KCl, 5 mM $MnCl_2$		
Substrate composition:		Initial 5 mM lactose, transferred; 6.5 mM fresh nucleotide sugar		
Cross flow period:		Only for last reaction step		
SpyC-LgtA	SpyT-agarose	UDP-GlcNAc	lactose	LNTII
SpyC-β4GalT	microgel	UDP-Gal	LNTII	LNnT
SpyC-α3,4FucT	SpyT-agarose	GDP-Fuc	LNnT	LNFPIII
Reaction (ii) Lewis^X-*t*Boc				
Approach: Defined intermediate reaction mix				
Buffer composition:		100 mM TRIS-HCl pH 7.5, 25 mM KCl, 5 mM $MnCl_2$		
Substrate composition:		5 mM acceptor & 6.5 mM nucleotide sugar for each reactor run		
Cross flow period:		Active for all steps		
SpyC-β4GalT	microgel	UDP-Gal	GlcNAc-*t*Boc	LacNAc-*t*Boc
SpyC-α3,4FucT	SpyT-agarose	GDP-Fuc	LacNAc-*t*Boc	Lewis^X-*t*Boc
Reaction (iii) Galili-*t*Boc				
Buffer composition:		100 mM TRIS-HCl pH 7.5, 150 mM KCl, 6 mM $MgCl_2$, 5 mM $MnCl_2$		
Substrate composition		1 mM GlcNAc-*t*Boc & 2,6 mM UDP-Gal		
Cross flow period:		Active for both strategies		
Approach A: One reactor module				
SpyC-β4GalT	microgel	UDP-Gal	GlcNAc-*t*Boc	LacNAc-*t*Boc
SpyC-α3GalT	microgel	UDP-Gal	LacNAc-*t*Boc	Galili-*t*Boc
Approach B: Precolumn for LacNAc-tBoc intermediate synthesis + reactor module				
SpyC-β4GalT	Ni^{2+}-IDA beads	UDP-Gal	GlcNAc-*t*Boc	LacNAc-*t*Boc
SpyC-α3GalT	microgel	UDP-Gal	LacNAc-*t*Boc	Galili-*t*Boc
Reaction (iv) Blood group A tetraose type VI				
Buffer composition:		100 mM TRIS-HCl pH 7.5, 25 mM KCl, 20 mM $MgCl_2$		
Substrate composition		1 mM GlcNAc-*t*Boc, 1.3 mM GDP-Fuc, 1.3 mM UDP-GalNAc		
Cross flow period:		Active for both strategies		
Approach A: One reactor module, Ni^{2+}-IDA beads				
SpyC-FutC	Ni^{2+}-IDA beads	GDP-fucose	lactose	2′-FL
SpyC-GTA	Ni^{2+}-IDA beads	UDP-GalNAc	2′-FL	BGA type VI
Approach B: One reactor module, Ni^{2+}-IDA beads, and microgels (Appendix)				
SpyC-FutC	Ni^{2+}-IDA beads	GDP-fucose	lactose	2′-FL
SpyC-GTA	microgel	UDP-GalNAc	2′-FL	BGA type VI

2.8.1. Analysis of tBoc-linked glycans via HPLC-UV analysis

Reaction samples were collected at defined time points and analyzed by HPLC-UV using an UltiMate 3000 system (Thermo Fisher Scientific, Waltham, MA, USA) equipped with a Silica-C18 column (MultoKrom 100–5 C18, 250 × 4 mm; CS Chromatographie, Langerwehe, Germany). Chromatograms were processed with Chromeleon 7.2.6 software (Thermo Fisher Scientific, Waltham, MA, USA). Separation was achieved with a polar mobile phase consisting of 15% acetonitrile (Roth, Karlsruhe, Germany) over 30 min at a flow rate of 1 mL min^{-1}. Detection of *t*Boc-linked sugars was carried out at 254 nm. Conversion and enzymatic activity were calculated from the ratio of acceptor to product peak areas at the respective time points. Here, volumetric activity ($U{\cdot}mL^{-1}$) was determined from the slope of the linear regression. Specific activity ($U{\cdot}mg^{-1}$) was subsequently calculated based on the protein concentration. One unit (U) was defined as the amount of product (μmol) formed by the enzyme per minute. An exemplary calculation was described earlier [7].

2.8.2. Analysis of APTS-labeled glycans via xCGE-LIF

Lactose-based glycans with a free reducing end were analyzed using multiplexed capillary gel electrophoresis with laser-induced fluorescence detection (xCGE-LIF) as reported before [43–46] with minor adaptations. Briefly, samples of the reactor feed, product, and waste effluents were labeled with APTS and purified using the glyXprep™ Glycan Labeling Kit PLUS (glyXera GmbH, Magdeburg, Germany), carefully following the kit's instructions. After labeling and post-labeling clean-up, the samples were appropriately diluted and analyzed on a GlycoDecoder™ system (glyXera GmbH, Magdeburg, Germany), based on a modified ("glyconeered") 16 capillary 3130xl Genetic Analyzer equipped with a 50 cm capillary array filled with POP-7™ polymer. The samples were electrokinetically injected and analyzed with a running voltage of 15 kV. Generated glycan data were analyzed with the glycoanalysis software glyXtoolCE™ (glyXera GmbH, Magdeburg, Germany), performing migration time alignment to the glyXalign GA4-S internal alignment standard (glyXera GmbH, Magdeburg, Germany) for peak annotation, and a relative quantification of glycans by normalization to the total peak area (TPA) of the respective sample, i.e., to % TPA.

For absolute quantification of glycans [47] during the LNFPIII synthesis, 3 aliquots of 1 μL of sample were each spiked with 1 μL of a 1 mM maltoheptaose solution (Fluka, Honeywell Research Chemicals, Morris Planis, NJ, USA) as an internal standard prior to the sample preparation and analysis described above, as a technical triplicate. Subsequently, glycan peak areas were first quantified relative to the peak area of the internal standard (i.e., to %IS), using glyXtoolCE™. The internal standard was then calibrated against lactose solutions of defined concentrations (0.01 mM – 5 mM), using linear regression. Finally, the linear regression was used to translate the relative peak areas of glycans (in % IS) into absolute concentrations (in mM).

2.8.3. Analysis of nucleosides and nucleotide sugars via CE-UV

Nucleotide sugars, including UDP-Gal, UDP-GalNAc, and GDP-fucose, nucleotides, including UDP and GDP, as well as nucleosides, including guanosine and uridine, were quantified by capillary electrophoresis with UV detection (CE-UV) [48]. Samples were prepared 1:1 mixed with 28 mM SDS, and, for quantification, para-aminobenzoic acid (PABA, 1 mM) and para-aminophthalaic acid (PAPA, 1 mM) served as internal standards. Product concentrations were determined from normalized peak areas relative to calibration curves of authentic standards. For detection, a 7100 CE system (Agilent Technologies, Santa Clara, CA, USA) allowed precise separation of individual samples. The system is equipped with OpenLAB CDS Chemstation Edition 01.07 software and a PVA-coated fused silica capillary (64.5 cm total length, 56 cm effective length, 50 μm ID) and a Diode Array Detector (DAD) (Agilent from Picometrics Technologies SAS, Toulouse, France). Samples were injected under vacuum (−0.7 psi or − 48 mbar, 10 s), and separated for 70 min at 20 kV (50 mM Borax decahydrate, 64 mM boric acid). Prior to analysis, capillaries were conditioned with 0.1 M NaOH, rinsed with water, and filled with running buffer. Detection was performed at 254 nm.

3. Results and discussion

3.1. Establishment of a continuous flow membrane reactor for glycan synthesis

In this study, the proof-of-principle of the continuous flow membrane reactor was demonstrated by the synthesis of glycan structures following different reactor strategies. Fig. 2 shows a sketch of the designed IEMR

module and its flexible operation modes, allowing a synthesis step of the aimed glycan molecule using immobilized GTs, a plain crossflow operation for the subsequent removal of unwanted side products, and even the simultaneous combination of both processes. This is possible by a unique design consisting of a central flow-through middle reaction compartment with the possibility to be filled with particulate enzyme carriers and two adjacent lateral compartments for feed and drainage of fresh and spent buffer solution separated from the middle compartment by a nanofiltration membrane each. This arrangement allows a controlled central flux in which substrates are reacted into products and a simultaneous, on-demand, crossflow of an independent buffer solution. The buffer crossflow can remove contaminants but also can gradually switch the pH and/or the ion matrix of the central solution carrying intermediate or end products. In this way, optimal conditions for subsequent reaction steps or final product formulation can be achieved. Further information on filtration design of the reactor is described in the supplementary information.

Combining several of these multi-purpose modules with multi-port valves and multiple precise piston pumps, an automated multi-step reaction system can be assembled which allows the flexible synthesis of different glycan structures. In this paper, we first describe the realization of the required preconditions, various GTs, suitable enzyme-loaded carriers, a multi-purpose reactor module, and the final automated setup. Afterwards, four proof-of-concept glycan syntheses with increasing complexity will be presented and discussed.

Towards this aim, glycosyltransferases were immobilized and embedded in the membrane separated reaction chamber of the reactor module. To this end, the syntheses of (i) LNFPIII and (ii) Lewis^X-*t*Boc in a sequential multiple modular reactor approach, as well as (iii) the Galili-*t*Boc and (iv) human blood group A tetraose type VI in a mixed enzyme reactor were demonstrated (Table 4 and Fig. 3). In short: (i) For the synthesis of lacto-*N*-fucopentaose III (LNFPIII) from lactose, every intermediate was synthesized in individual reactor modules, and the intermediates were transferred to the next reactor, respectively. First, SpyC-LgtA was used for the formation of lacto-*N*-triose (LNTII) with UDP-GlcNAc. Second, LNTII was converted to lacto-*N*-neotetraose (LNnT) by SpyC-β4GalT and UDP-Gal. Finally, lacto-*N*-fucopentaose III (LNFPIII) was formed by the addition of fucose from GDP-fucose by SpyC-α3,4FucT. (ii) Synthesis of Lewis^X from GlcNAc-*t*Boc followed a similar sequential approach. Here, first, LacNAc-*t*Boc was synthesized from GlcNAc-*t*Boc. Second, pre-synthesized LacNAc-*t*Boc was used for the formation of Lewis^X-*t*Boc by SpyC-α3,4FucT and GDP-fucose. While the first two strategies demonstrated sequential syntheses of glycans, using all enzymes in separate reactor modules and reaction steps, in the next two approaches, the syntheses of the intermediate and the final product were performed in the same reactor, involving all relevant enzymes. (iii) For the synthesis of the Galili-*t*Boc, starting from GlcNAc-*t*Boc, the intermediate LacNAc-*t*Boc was synthesized by SpyC-β4GalT and UDP-Gal. Subsequently, Galili-*t*Boc was formed from LacNAc-*t*Boc by SpyC-α3GalT and UDP-Gal. (iv) Lactose was converted to 2′-fucosyllactose (2′-FL, H-antigen VI) by FutC and GDP-fucose. Continuing, attachment of GalNAc from UDP-GalNAc by SpyC-GTA led to the formation of BGA (blood group A tetraose type VI) antigen.

Noteworthy, both, free and *t*Boc-labeled glycans, namely GlcNAc-*t*Boc and lactose, were employed for different synthesis strategies. While the -*t*Boc group enables fast and convenient, direct detection at 254 nm via HPLC, allowing high-throughput analysis of multiple samples, APTS labeling provides a highly sensitive and precise method for xCGE-LIF-based glycan analysis in ultra-high-throughput but requires additional sample preparation before analysis. Using both glycan types within the reactor system further allows to demonstrate that the presence of the label does not influence the enzymatic synthesis and does not affect reactor performance, including membrane retention behavior. Notably, the higher molecular weight of the sugars bearing a -*t*Boc linker may enhance the retention of both substrate and product, thereby improving the efficiency of the separation process. Importantly, the *t*Boc linker can

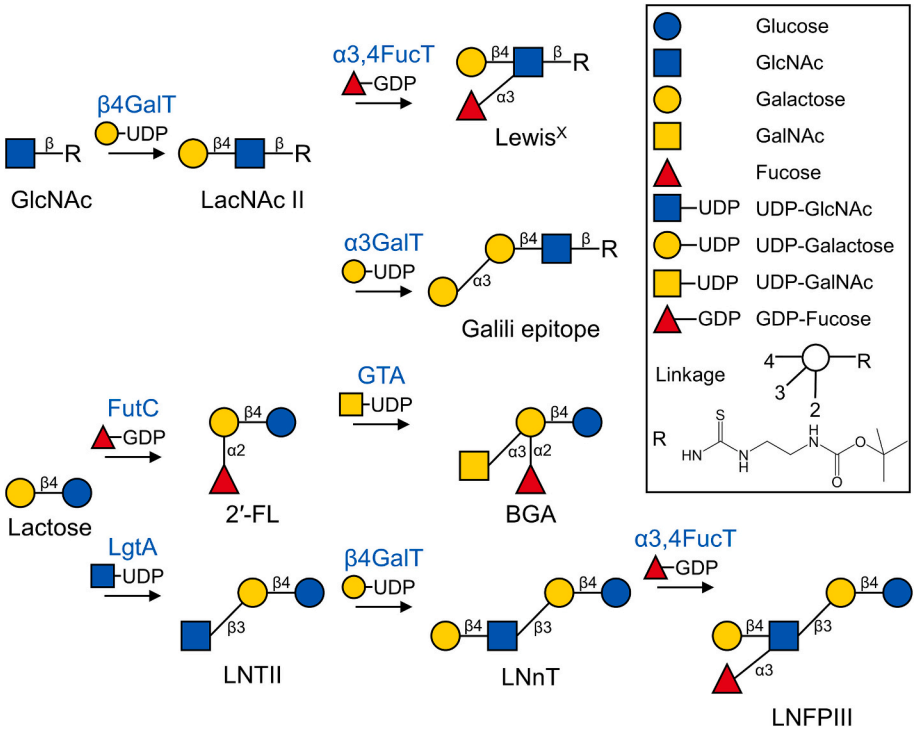

Fig. 3. Overview of synthesized glycans and intermediates. Four different syntheses are depicted: Synthesis of Lewis^X-*t*Boc and the Galili-*t*Boc from GlcNAc-*t*Boc with LacNAc-*t*Boc as an intermediate, BGA and LNFPIII, starting from lactose with 2′-FL or LNTII and LNnT as intermediates, respectively. Visualization is in accordance with the symbol nomenclature for glycans (SNFG [51]) and explained in the upper right box. Enzymes are depicted in blue and introduced above the arrows, together with respective nucleotide sugars. Selected glycans carry a *t*Boc linker (−R); the structure is visualized in the upper right box. Abbreviations of enzymes, nucleotide sugars and glycans are listed in Table S1 – Table S3.

be removed afterwards to bind the respective glycans to proteins via the free amino group to potentially synthesize neoglycoproteins [49,50].

3.2. Characterization of microgel properties for use in reactor and immobilization of glycosyltransferases

For the application of microgels as carriers for the automated glycan synthesis in a flow reactor, it is essential to investigate their mechanical and diffusion properties to ensure good stability and suitable substrate/product diffusion during the use in the reactor. Previous studies investigated the microgel's pore size and permeability [7], here, the spectrum of methods was extended to gain further insight in the properties of the microgels.

First, nanoindentation and micropipette aspiration measurements were performed to investigate the mechanical properties. During nanoindentation only approximately 1 µm of the microgels' surface is indented, while micropipette aspiration is used to aspirate large parts of a microgel. Thus, the Young's moduli determined using both techniques may vary, especially when the microgels are inhomogeneous with respect to their chemical crosslinking throughout the network. The results of the characterization of the microgels' mechanical properties are shown in Fig. 4.

Firstly, both nanoindentation and micropipette aspiration results are very similar, indicating homogeneous crosslinking of the reactive PEG pre-polymers. Secondly, all microgels range from roughly 15 to 40 kPa, which is comparable to other PEG-based microgels [52]: The microgels are soft but stable enough to be employed in the flow reactor.

Fluorescence recovery after photobleaching (FRAP) measurements were performed to determine the diffusion coefficient of 4 kDa FITC-dextrans in the core of the microgels, and in the free solution as reference. Confocal laser scanning microscopy (CLSM) images of the fluorescence recovery are shown in Fig. 4C. Overall, the microgels exhibit values of approximately 70 $\mu m^2\ s^{-1}$ while the free FITC-dextrans in solution have a value of around 120 $\mu m^2\ s^{-1}$ (Fig. 4B). The microgels have a diffusion coefficient of circa two-thirds of that of the solution, which shows that the diffusion is only restricted slightly. Since the substrates and products vary between approximately 200 and 900 g mol^{-1}, it can be expected that their diffusion is even better than 70 $\mu m^2\ s^{-1}$ for the 4000 g mol^{-1} dextran. In conclusion, both the investigation of the mechanical properties as well as the diffusion properties confirm the suitability of the microgels as carriers for enzymes in the automated glycan synthesis in a flow reactor. A more detailed discussion of the nanoindentation, micropipette aspiration and FRAP measurements can be found in the Supporting Information (Fig. S1 – S3).

While better understanding and comparison of microgel and SpyT-agarose properties would be beneficial for understanding of matrix embedment within the reactor, an in-depth characterization of the commercially available maleimide-activated agarose was beyond the scope of this publication. Immobilization of enzymes was further confirmed via confocal laser scanning microscopy (Fig. S4).

After the detailed characterization of the microgels, they were synthesized containing enzymes to be used in the flow reactor. For the immobilization of glycosyltransferases in microgels, eight previously established immobilization strategies [7] were applied in this study. The immobilization of SpyC-β4GalT and SpyC-α3GalT has been described earlier [7], the repertoire of immobilized glycosyltransferases was extended with novel immobilization of SpyC-GTA and SpyC-α3,4FucT. Because the amount of non-immobilized enzyme cannot be determined during droplet-based microfluidic encapsulation, an immobilization efficiency of 100% was assumed. This likely underestimates the actual enzyme activity, meaning the system may perform better than reported. The post attachment approaches yielded microgels with high immobilization efficiency for SpyC-α3,4FucT between 60 and 70% for the VS immobilizations and above 80% for the SpyT immobilizations. SpyC-α3GalT immobilized as SpyT-L had an immobilization efficiency of 90%, and while the efficiencies for the VS methods for SpyC-α3GalNAcT ranged from 85 to 90%, the SpyT methods were close to 100% (Table S4). Even though the efficiency depends on the immobilization technique and enzyme, the enzyme immobilization in microgels is highly efficient. As shown in Fig. S5, for SpyC-GTA, the cov-L approach, where the enzyme is incorporated into the microgels during the synthesis and forms covalent bonds with the free VS groups through Michael-type addition reaction, performs best. Therefore, the cov-L type microgels containing SpyC-GTA was used for the presented experiments. The activity of microgel immobilized SpyC-α3,4FucT was strongly decreased in comparison to the free enzyme (Fig. S5), therefore, SpyTag-

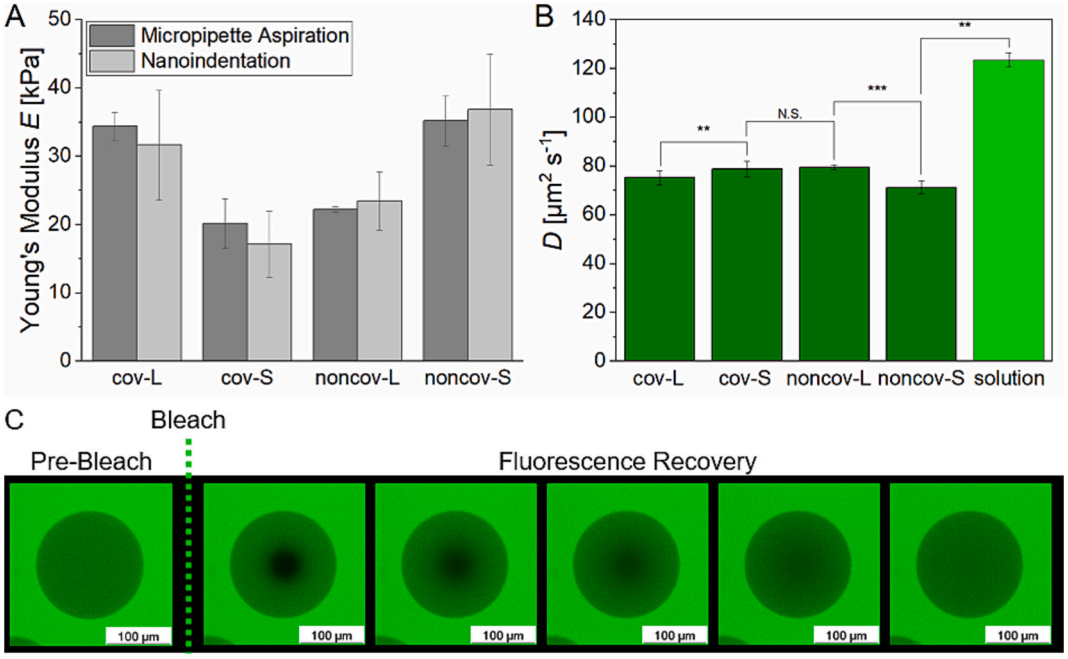

Fig. 4. Results for mechanical properties (A) and diffusion properties (B) of the cov and noncov type microgels. Confocal laser scanning microscopy images (C) show the fluorescence recovery during fluorescence recovery after photobleaching experiments.

agarose immobilized SpyC-α3,4FucT version was used for further process.

3.3. Enzymatic glycan synthesis with reactor-embedded immobilized enzymes

Understanding of the reactor environment and characterization of immobilized glycosyltransferases now offer the possibility to embed enzymes within the reactor to perform automated glycan synthesis. Based on different synthesis strategies, deeper insights into the performance of the reactor were gained. As described in Table 4, different immobilization strategies were applied for embedment of enzymes in the reactor, namely microgels, SpyT-agarose and Ni^{2+}-IDA beads. The immobilization methods were selected based on the enzymatic activity. Furthermore, the application of different immobilization strategies should demonstrate the versatility of the reactor for different embedded immobilized enzymes. Further information on immobilization efficiency is given in Fig. S4 – S6.

Different synthesis strategies were applied as essential key investigative experiments to gain insights into the performance of the reactor prototype. Here, exemplary syntheses of LNFPIII, BGA, $Lewis^X$ and Galili were performed in order to demonstrate the versatility of the MiRAGE platform prototype across multiple modes of operation. These variations included differences in immobilization methodology, reactor setup, the use of cross-flow operation and the number of immobilized enzymes within the reactor. By applying these distinct strategies, we illustrate that the reactor system can accommodate different process designs depending on the requirements of the enzymatic cascade. At the same time, these approaches allowed us to gain insights into by-product formation, the uniformity of flow-synthesis, as well as enzyme (and immobilization) compatibility. In particular, exemplary synthesis of LNFPIII investigated formation of by-products, the role of reactor integrity and transfer of intermediate syntheses. For the synthesis of $Lewis^X$, freshly prepared intermediate was used rather than transferring the entire reaction mixture. This enabled the use of defined substrate concentrations and thereby facilitate quantitative modeling of the reaction system. Synthesis of Galili-*t*Boc and BGA with reduced amounts of immobilized enzymes highlighted constraints in catalytic capacity within the reactor and thereby providing insights into the system performance.

At this stage, these experiments were not intended to establish a complete preparative workflow including final product isolation, but rather to evaluate the reactor concept, its operational modes, and the feasibility of automated multistep glycan synthesis with immobilized enzymes. Accordingly, downstream purification of the final glycans was not investigated as a dedicated study objective in the present proof-of-concept work.

3.3.1. Sequential flow reactor operation for synthesis of LNFPIII

Separation of individual synthesis steps to different reaction modules offers the advantage of having precisely controlled reaction environments and distinct monitoring of intermediate product production. Therefore, in the first two examples of glycan synthesis applying the developed microgels and EMRs, one reaction module is applied for each single step towards the synthesis of the final product. In the case of LNFPIII the synthesis was performed in three distinct steps applying operation mode A (cf. Fig. 2) within individual reactor modules. The primary objective of this initial establishment of the reactor was to evaluate the reactor operation mode. To this end, a parallel one pot reaction was conducted outside the reaction system in which the respective nucleotide sugars and immobilized enzymes of the reaction mixtures were combined (Fig. S12). The formation of target glycans along with potential by-products was subsequently analyzed.

After recovery of the intermediate product fraction after synthesis within the first EMR, the whole mixture is supplemented with the specific nucleotide sugar as well as cofactors for the next glycosyltransferase reaction, and subjected to the following reactor module (Fig. 5A). The initial reaction mixture consisted of lactose, UDP-GlcNAc essential co-factors, and buffer salts, and was transferred to the next reactor run for subsequent conversion of the intermediates. SpyT-agarose-immobilized SpyC-LgtA was used to synthesize LNTII from lactose and UDP-GlcNAc. Next, following the LNTII synthesis, LNnT was synthesized in the microgel SpyC-β4GalT reactor module by the addition of UDP-Gal to the intermediate reaction solution. Finally, LNFPIII was synthesized from LNnT by reactor-embedded SpyT-agarose-immobilized SpyC-α3,4FucT and GDP-fucose (Fig. 5A).

For each EMR reaction step, a sample of the respective reaction mixture (MM) and synthesis mixture (RX) was collected for glycan analysis via xCGE-LIF (Fig. 5B, Fig. S12). The conversion of lactose to the final product LNFPIII was accomplished in three consecutive steps: lactose ➔ LNTII ➔ LNnT ➔ LNFPIII. For each reaction step, the absolute glycan yield was determined, allowing calculation of both relative and total conversion rates. The relative conversion refers to the conversion of the respective intermediate, excluding unconverted precursor glycans, whereas the total conversion represents the proportion of the respective glycan relative to all remaining, non-converted glycans in the reaction mixture.

The initial reaction mixture (MM1) contained 5.2 mM lactose and was transferred through the individual reaction modules. In the first step, lactose was converted to LNTII by SpyT-agarose immobilized SpyC-LgtA and UDP-GlcNAc. The total glycan concentration after the synthesis was 4.1 mM with 36% LNTII, indicating a certain loss of glycans during the synthesis (RX1). Next, the LNTII reaction was supplemented with UDP-Gal (MM2) and transferred to a microgel-immobilized SpyC-β4GalT reactor module for synthesis of LNnT. After the reaction, a decline of the total glycan concentration to 2.5 mM was observed with a LNnT yield of 39% (RX2). Interestingly, the LNnT yield exceeded the initial relative amount of 36% LNTII. This could indicate leakage of SpyC-LgtA from the first synthesis step and transfer (together with UDP-GlcNAc) to reactor 2, leading to further conversion of lactose to LNTII (7% relative content of LNTII in RX2). With this, overall, 39% from 46% of LNTII were used for LNnT synthesis (84.8% synthesis yield). For the final reaction step, RX2 was supplemented with GDP-Fucose (MM3) and transferred to a SpyT-agarose immobilized SpyC-α3,4FucT reactor module for synthesis of LNFPIII. Noteworthy, for this synthesis the mode of operation was switched to the cross-flow (operation mode C, c.f. Fig. 2). A strong decline in total glycan concentration to 0.2 mM was observed, indicating an inefficient retention of the selected membrane. Leakage of enzymes from previous reactor modules also impacts the third reactor: the 6% LNTII in RX2 were converted increasing the ratio of 39% LNnT to 45% during the preparation of MM3. After the third reactor run, LNTII is detectable again, and the combined content of 50% LNnT and LNFPIII in RX3 is higher than the 45% LNnT in MM3. Taken together, this indicates that SpyC-LgtA and SpyC-β4GalT appear to leak to some extent. Despite the leakage of enzymes and decline in total glycan yield, LNFPIII was synthesized from overall 50% LNnT to 36% yield (conversion rate 72%).

These findings also underline that the present reactor configuration cannot yet be regarded as a final purification system for isolated glycan products. In the current proof-of-concept setup, the crossflow operation was primarily assessed as an integrated process-conditioning step for buffer exchange and partial removal of low-molecular-weight side components. A meaningful evaluation of preparative end-product purification was not realistic at this stage, because the achieved product amounts were still too low and membrane selectivity was not yet sufficient for representative isolation studies.

Noteworthy, it was observed that the yield of target glycans was higher in the one-pot reactions (Fig. S12), which can be attributed to the extended reaction time compared to the shorter residence time in the reactor system. Nevertheless, the reactor setup, particularly due to the (mostly successful) retention of enzymes, resulted in a markedly lower formation of undesired by-products (Fig. S12). Notably, although the

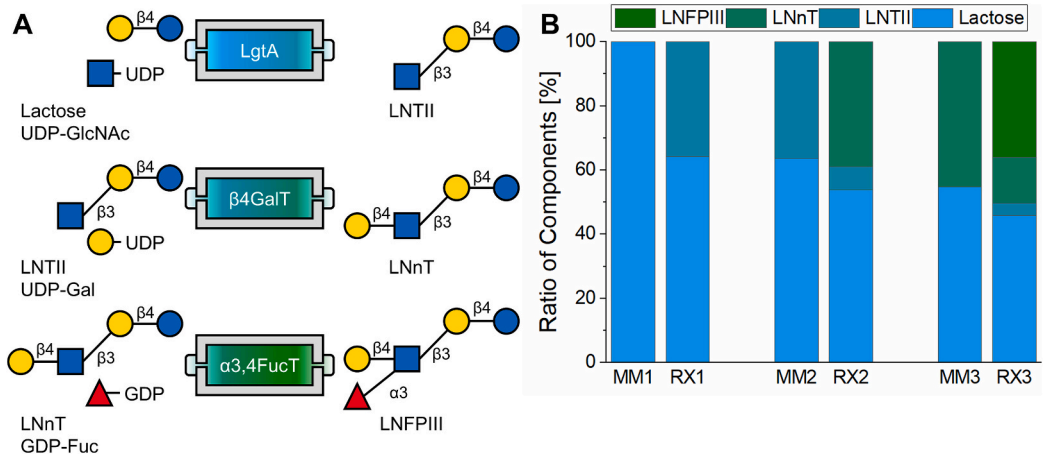

Fig. 5. A) Synthesis of lacto-*N*-fucopentaose III (LNFPIII) applying three distinct reactor modules. Towards the synthesis of LNFPIII, the different reaction steps are split into three reactor modules: The intermediate reaction mix was transferred through the next module, together with additional nucleotide sugar and buffer components. First, the initial reaction mix containing lactose and UDP-GlcNAc was transferred through a SpyT-agarose-immobilized SpyC-LgtA reactor module. The reaction, containing LNTII as well as non-processed lactose, was subsequently transferred to the second reactor module, containing microgel immobilized SpyC-β4GalT, together with UDP-Gal, yielding LNnT and residual intermediates. Finally, GDP-fucose was added to the reaction and transferred through reactor-embedded SpyT-agarose-immobilized SpyC-α3,4FucT for recovery of the final product LNFPIII. B) Glycan ratio of individual reaction mixtures (MM) and syntheses mixtures (RX). Reaction mixture for each reaction was sampled before and after synthesis. MM1, RX1: SpyC-LgtA reaction; MM2, RX2: SpyC-β4GalT reaction; MM3, RX3: SpyC-α3,4FucT reaction.

total glycan amount decreased, we were still able to demonstrate efficient synthesis of the individual glycans, reaching 85% for LNnT and 79% for LNFPIII, calculated relative to their respective precursor glycans.

To assess whether the observed formation of LNTII from lactose is consistent with the applied reactor configuration, a simplified plug-flow reactor (PFR) model assuming first-order, substrate-limited kinetics was considered. For the enzymatic membrane reactor operated at a volume of 0.6 mL and a flow rate of 10 μL min^{-1}, the resulting mean residence time is $\tau = V/Q \approx 60$ min. For a first-order reaction in a PFR, the concentration profile is given by $C_{out}/C_{in} = \exp(-k\tau)$, yielding a conversion $X = 1 - \exp(-k\tau)$. A benchmark conversion of 50% at an inlet concentration of 5 mM would therefore require $k = \ln(2)/\tau \approx 0.012\,min^{-1}$. Under substrate-limited conditions, the corresponding effective volumetric activity follows directly from $a_V = kC_{in}$. With $C_{in} = 5$ mM, this results in an activity requirement of $a_V \approx 0.012 \times 5 = 0.058\,U\,mL^{-1}$, corresponding to approximately 58 mU mL^{-1}. In the present case, the apparent yield of LNTII derived from precursor conversion was 36%, corresponding to $C_{out}/C_{in} = 0.64$. From the PFR relation, this translates into an effective rate constant of $k = -\ln(0.64)/60 \approx 0.0074\,min^{-1}$. Using $a_V = kC_{in}$ at $C_{in} = 5$ mM yields an effective reactor activity of $a_V \approx 0.0074 \times 5 = 0.037\,U\,mL^{-1}$, i.e. approximately 37 mU mL^{-1}.

Standard batch assays of the corresponding SpyC-LgtA immobilized on SpyTag-functionalized agarose yielded a volumetric activity of approximately 123 mU mL^{-1} under enzyme-optimal conditions (Table S7). In the sequential, buffer-continuous reactor setup, however, no intermediate buffer exchange was possible, necessitating a compromise pH to maintain compatibility with downstream glycosyltransferase steps.

The applied glycosyltransferases exhibit distinct optimal reaction conditions, particularly with respect to pH, therefore, a systematic screening of reaction parameters was performed for all enzymes used in this study prior to immobilization and reactor implementation [8]. Previous studies on multi-enzyme glycosylation cascades have shown that one-pot systems generally require the selection of a compromise pH that ensure compatibility across all participating enzymes while maintaining sufficient catalytic activity [7,8,53]. In these cases, the selected pH is typically determined by the requirements of the least stable or rate-limiting enzymes within the cascade. The range of residual enzymatic activity was hereby measured between a pH of 5.5 and 10. [8,53] Importantly, under the compromised pH conditions used, all glycosyltransferases retained measurable catalytic activity, even though the selected pH buffer system did not necessarily correspond to their individually determined optima. The selected reaction conditions represent a practical balance between maintaining enzymatic activity across the cascade and ensuring operational compatibility within the multi enzyme synthesis.

As a consequence, the effective in-reactor activity of the carrier is expected to be substantially lower than its standard assay activity. Taken together, the observed LNTII formation in reaction (i) falls well within the expected performance range of a residence-time-limited PFR operated under non-optimal but process-integrated conditions.

For the subsequent elongation of LNTII to LNnT, a direct estimation of the effective in-reactor activity using the PFR model is not possible, due to uncertainties in the initial substrate concentration in this reaction. Nevertheless, the observation of quantitative conversion suggests that the effective activity of the immobilized SpyC-β4GalT under reactor conditions was sufficiently high to fully process the available substrate. This behavior is consistent with the comparatively high standard assay activity of the SpyC-β4GalT carrier (≈132 mU mL^{-1} under optimal conditions) and indicates that this reaction step was not rate-limiting within the modular sequence.

In addition to the intrinsically high assay activity, the full conversion of LNTII may also reflect more favourable reaction conditions for the immobilized SpyC-β4GalT in the reactor environment. In particular, the pH selected as a compromise for sequential operation is closer to the reported pH optimum of SpyC-β4GalT than to that of the upstream SpyC-LgtA, potentially resulting in a smaller relative activity loss compared to the first reaction step. Moreover, a lower apparent K_M of SpyC-β4GalT for LNTII compared to the initial lactose substrate would reduce the impact of substrate limitation, such that the reaction rate remains near saturation even at sub-millimolar LNTII concentrations.

By contrast, the final transformation of LNnT to LNFPIII reached an apparent yield of 80%, indicating partial conversion within the available residence time. In this case, the observed yield is consistent with a lower effective activity of the immobilized α3,4-fucosyltransferase relative to SpyC-β4GalT. While standard batch assays of the corresponding carrier report volumetric activities on the order of 100–120 mU mL^{-1} under

optimal conditions (Table S7), the effective in-reactor activity is expected to be reduced due to the combined effects of lower substrate concentration and pH compromise. Consequently, the fucosylation step becomes moderately rate-limiting, leading to partial accumulation of LNnT as an intermediate.

Taken together, the distinct conversion levels observed for the three consecutive steps in reaction (i) can be rationalized by the interplay of residence time, substrate availability, intrinsic enzyme activity, and the deviation of reactor conditions from individual assay optima. The quantitative conversion of LNTII to LNnT highlights the robustness of the SpyC-β4GalT-catalyzed step under continuous-flow conditions, whereas the incomplete upstream and downstream conversions reflect the expected performance of immobilized glycosyltransferases operated under process-integrated, non-optimal conditions. Noteworthy, the activities of the immobilized enzymes vary between batches. Therefore, enzymes were verified prior to each run, even if variations in activity can be observed in contrast to previous data [7,8]. Enzyme activity was determined as described in Table 2 using shorter substrates to confirm catalytic activity. The assays do not fully replicate the reactor conditions, but serve as a good hint for assessment of enzymatic activity.

3.3.2. *Sequential synthesis of Lewis^X*

Incomplete conversion of intermediates results in the accumulation of these glycans in every following fraction, including the final product mixture. Furthermore, the loss of total glycan complicates the analysis of individual reaction steps. Thus, the targeted concentration ratio of acceptor glycan to nucleotide sugar donor will not be achieved. Therefore, the next approach was performed using a defined reaction mixture for every individual step. Here, previously synthesized GlcNAc-*t*Boc and LacNAc-*t*Boc were used for the individual reaction steps, respectively. To monitor the performance in the reactor over time, fractions were collected during the whole synthesis step and analyzed for glycan and nucleotide sugar quantities. Furthermore, operation parameters of the controlling ÄKTA™ device were analyzed. First, LacNAc-*t*Boc was synthesized in a microgel-immobilized SpyC-β4GalT reactor module from GlcNAc-*t*Boc and UDP-Gal (Fig. 6A). Next, a buffer containing a defined concentration of LacNAc-*t*Boc and GDP-fucose was prepared to synthesize Lewis^X-*t*Boc in a SpyT-agarose-SpyC-α3,4FucT reactor module (Fig. 6E). HPLC chromatograms and calculation of glycan concentration is given in Fig. S9 and S10 as well as Table S9 and S10.

Starting from 5 mM substrate acceptor glycan, glycan yield and byproducts over the time of the reactor run were investigated. For both reaction steps, a sequence of 200 min pure reaction mode followed by 300 min combined diafiltration/reaction mode (cf. Fig. 2A and C) was applied. At a feed flow rate of 10 μL min^{-1} this resulted in a treated volume of 2 mL in pure reaction mode, and 3 mL in the combined reaction/diafiltration mode. In total this summed up to the 5 mL sample feed provided in a 5 mL injection loop at the beginning of the experiment.

The online monitoring of the ÄKTA system allows the sequential operating concept (reaction mode followed by combined reaction/diafiltration mode) to be reconstructed directly from the recorded volume, pressure, conductivity, and UV signals (Fig. 6B & F), ÄKTA real time monitoring is exemplary described for Lewis^X synthesis (Fig. 6F). The main experiments start by switching the feed flow in a way that it passes the 5 mL injection loop containing the reaction mixture. The reactor is fed at 10 μL min^{-1}; fractions are collected every 200 μL, i.e., every 20 min. As indicated by the marked periods a–d, the conductivity and UV–Vis sensor signals as well as the collected samples start in period a, where the initially present high-salt equilibration buffer is displaced. This period lasts for about 1.6 mL (8 fractions, fraction 2–10, because the first fraction is taken already during equilibration, the time point 0 mL corresponds to fraction 2). After fraction 10 period b starts with a length of 10 fractions (2 mL) up to fraction 20. Here, a high product yield of above 4 mM was detected. This period b corresponds to the 200 min in which the module is operated in plain reaction mode. The subsequent segment c corresponds to the combined reaction/diafiltration mode, corresponding with the application of the diafiltration crossflow at 40 μL min^{-1}. Because this diafiltration flow simultaneously enters and leaves the central compartment, the residence time of the axial flow in this compartment stays at around 60 min (600 μL volume and 10 μL min^{-1} feed flow). Period c could be maintained for an additional 3.0 mL (≈ 300 min, fractions 20 to 35), thereby exhausting the complete 5 mL loop content. Finally, period d indicates the return to the original high-salt buffer once the sample loop is fully flushed. Consequently, the UV signals sharply drop in period d and the conductivity turns back to its original value.

The periods highlight a systematic time/volume offset (~1.6 mL ≈ 160 min ≈ 8 fractions) between operational switching events and their appearance in the outlet-side sensor signals (conductivity and UV), caused by the residence time of the reactor, tubing, and in-line detectors. In contrast, the pressure sensor responds essentially instantaneously to changes in operating mode, so the onset of diafiltration mode is visible immediately in the pressure traces, whereas the corresponding change in conductivity/UV is only observed after the delay caused by passing the reactor volume. This offset of around 6–8 fractions between the visibility of the diafiltration mode in pressure (at fraction 14) and UV–Vis signal (fraction 20) is marked by the black arrow indicated “A”. The double arrow indicated “B” delineates the section of the pressure signal during which the diafiltration stream is applied and the reaction mixture from the sample loop is actually present in the reactor. This section typically manifests by slightly increased pressures compared to the pressures resulting during the following section with diafiltration but only buffer being pumped through the central compartment. A periodic oscillation of the pressure course within a broad band originating from piston-pump pulsation is removed by applying a LOESS-Filter (Locally Estimated Scatterplot Smoothing) with the OriginPro 2025b software resulting in pressure levels of 0.45 MPa in the in the DF compartment (sample pressure) and 0.28 MPa in the central compartment (PreC pressure) between samples 10 and 20 and pressures of 0.37 MPa and 0.18 MPa between samples 20 and 35. The initial phase operated at pure reaction mode shows a sample pressure of practically zero, because no transmembrane pressure is needed to force DF buffer through the membranes. The low PreC pressure indicates the low pressure drop within the microgel packed bed, when the feed flow of 10 μL min^{-1} is pumped through. When the DF flow of 40 μL min^{-1} is switched on, sample pressure directly jumps to about twice the PreC pressure, which is also strongly increased. The reason is, that the sample pump has to deliver the required transmembrane pressure for the passages of the DF flow through the upper and lower membrane. Fig. 6C-F shows the results of the analysis of the collected fractions, only the samples of the periods b and c are plotted, because only these represent the synthesis and in situ contaminant removal efficiencies during obtained by the two operation modes.

Fig. 6 C & D and G & H show the molarity of substrates, products and by-products of the two-step synthesis of Lewis^X. First, the effluent concentrations of the first reactions step, the synthesis of LacNAc-*t*Boc from GlcNAc-*t*Boc and UDP-Gal (Fig. 6C) is described. It clearly shows that the conversion rate of GlcNAc-*t*Boc to LacNAc-*t*Boc changed between the different periods. While the concentration of the LacNAc-*t*Boc increased up to 3.5 mM during the plain reaction mode of operation (period b, fractions 10–20), it quickly decreased after starting the diafiltration flow to below 1 mM (period c, fractions 20–35). The strong decline is caused by an unfavorable distribution profile of the reactants during period c. Due to the diafiltration flow transferring the membranes perpendicularly, the reactants are not evenly distributed across the channel height when flowing through the central compartment, but accumulate in the lower membrane area while the upper membrane area becomes depleted of reactants. As a result, a larger proportion of the immobilized enzyme remains unused in the upper area and the achieved conversion rate decreases. In addition, a certain portion of the product can also permeate through the lower membrane, which also reduces the

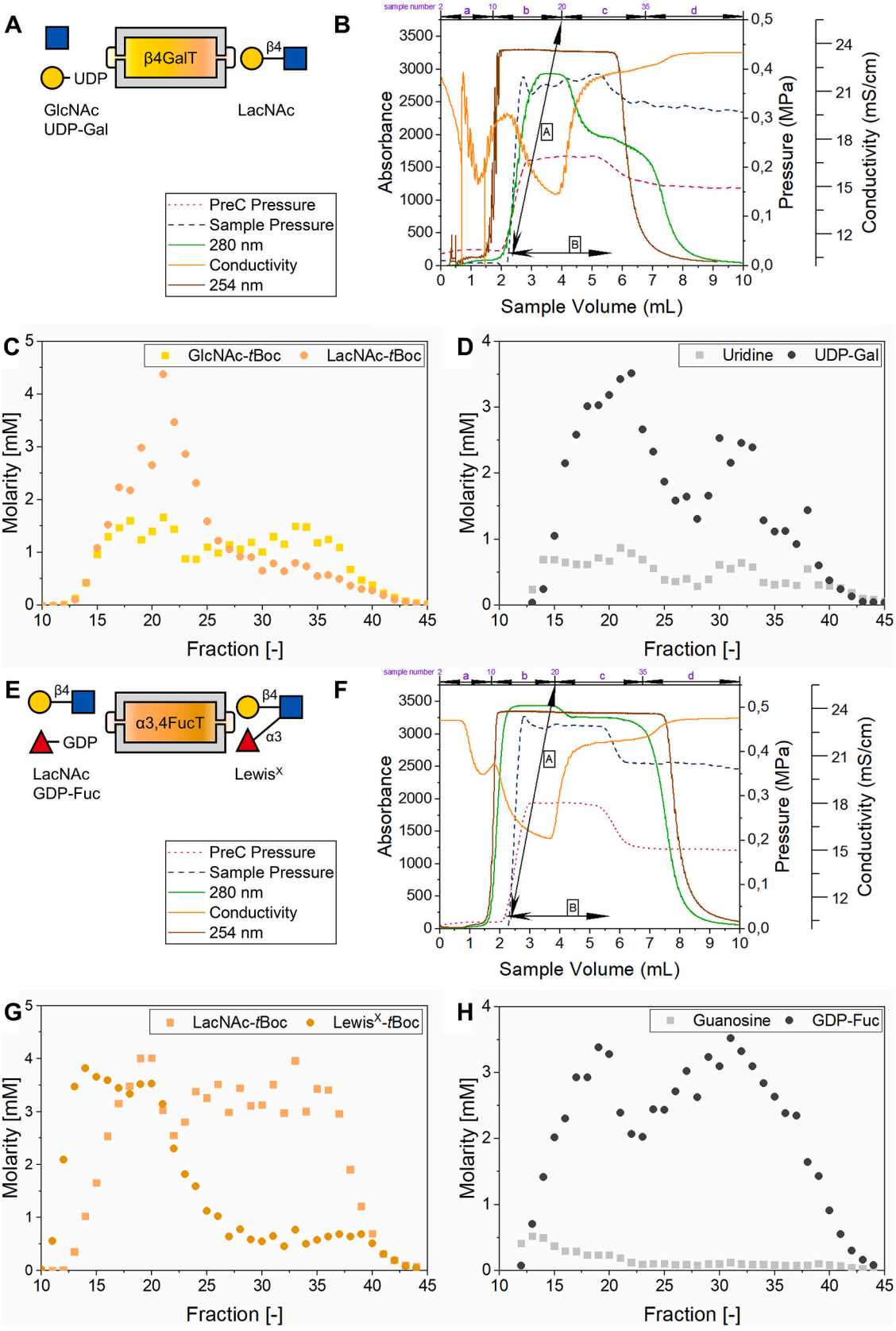

(caption on next page)

Fig. 6. Sequential synthesis of Lewis^X-*t*Boc from GlcNAc-*t*Boc via two reactor modules. In a first step, LacNAc-*t*Boc was synthesized from GlcNAc-*t*Boc (A – D), followed by the second synthesis step, using fresh reaction buffer, for the synthesis of Lewis^X-*t*Boc from LacNAc-*t*Boc (E – H). For every reaction, a fresh reaction mix, containing the acceptor glycan, nucleotide sugar, and buffer compounds, is used. A) First, GlcNAc-*t*Boc together with UDP-Gal was used to synthesize LacNAc-*t*Boc by reactor embedded SpyC-β4GalT. B) Online monitoring trace of an ÄKTA-controlled IEMR experiment operated in a sequence of plain reaction and combined reaction/diafiltration mode. Recorded signals include pumped volume through the central compartment, pressure in the packed reaction chamber (PreC pressure), pressure in the diafiltration (DF) compartment (sample pressure), conductivity, and UV absorbance at 254 nm and 280 nm. The marked periods a – d indicate the characteristic phases of the run: (a) displacement of the initial high-salt equilibration buffer and establishment of the reaction mixture in the flow path; (b) operation in pure reaction mode; (c) operation in combined reaction/diafiltration mode, with an additional DF crossflow applied via the sample pump; and (d) return to the high-salt buffer after exhaustion of the 5 mL injection loop, reflected by a drop in UV and recovery of conductivity. The meanings of the double arrows A and B are explained in the main text. C-D) Step1: Synthesis of LacNAc-*t*Boc from GlcNAc-*t*Boc and UDP-Gal. Molarity of the substrate GlcNAc-*t*Boc (yellow square) and the product LacNAc-*t*Boc (orange sphere), analyzed by HPLC-UV (C) nucleotide sugar UDP-Gal (black sphere) and the Fast-AP degradation product uridine (gray square), analyzed by CE-UV (D). Applying each a sequential operation with pure reaction mode (fractions 10 to 20) followed by a combined reaction/diafiltration mode (fractions 20 to 35). E) Subsequently, a fresh buffer, containing LacNAc-*t*Boc and GDP-Fuc was used to synthesize Lewis^X-*t*Boc by a reactor embedded SpyC-α3,4FucT. F) Online monitoring was performed as described in B). G – H) Step 2: Synthesis of Lewis^X-*t*Boc from LacNAc-*t*Boc and GDP-Fuc. (C) Molarity of the substrate LacNAc-*t*Boc (orange square) and the product Lewis^X-*t*Boc (brown sphere), analyzed by HPLC-UV (D) nucleotide sugar GDP-Fuc (black sphere) and the Fast-AP degradation product guanosine (gray square), analyzed by CE-UV. Mode of operation was performed as described in C – D).

concentration measured in the effluent. Looking at the reactant GlcNAc-*t*Boc, it shows that, after a short delay, the concentration of GlcNAc-*t*Boc stayed more or less constant around 1.5 mM during period b, matching the expectation that about 70% of the original concentration of 5 mM in the feed is consumed by the synthesis of LacNAc-*t*Boc. Interestingly, after a small drop, the concentration stayed at this level also in period c, when the diafiltration flow was switched on. It might have been expected, that due to the reduced transformation into LacNAc-*t*Boc, the concentration of GlcNAc-*t*Boc should show a strong increase in this period. However, this trend is compensated by the permeation of the molecule through the membrane.

The second reactant, UDP-Gal, also shows an initial increase during period b, reaching up to 3.5 mM, correlating with the highest LacNAc-*t*Boc concentration at fraction 21 (Fig. 6D). Compared to GlcNAc-*t*Boc the highest concentration is about 2 mM higher, however, this could easily be explained by the higher feed concentration of this reactant (6.5 mM compared to 5 mM). In period c, also UDP-Gal shows a sharp drop followed by a temporary increase before leveling at around 1 mM. The reason for the temporary increase, which to a smaller degree can also be seen for GlcNAc-*t*Boc, is not fully understood. However, we know from pure diafiltration experiments that the accumulation of reactants at the membrane surface increases its retention behavior. The slowly forming accumulation layer during the first few hours of period c may therefore be the reason that less UDP-Gal is lost into the permeate and the concentration in the retentate shows a temporary increase. The waste product uridine is formed by the enzymatic degradation of UDP by the dissolved enzyme FastAP, which is added to the reaction mix. During period b uridine increases up to around 1 mM, showing that the degradation of UDP is not complete during the residence time in the reactor. Switching to period c, the concentration of uridine drops by about 50%, again with a temporary increase in the middle of period c. Nevertheless, this reduction of small contaminants by about 50% in period c shows the proof-of-concept of in situ contaminant removal by the combined reaction/diafiltration mode.

The second reaction step transformed LacNAc-*t*Boc and GDP-fucose into Lewis^X-*t*Boc and GDP (Fig. 6E-H). The latter was simultaneously reduced to guanosine by dissolved FastAP. Looking at the concentrations of educts and products analyzed with fractions 10 to 35 (period b and c) it shows, that although conducted in a separate reactor module the second reaction follows the same trends that has been described for the first reaction step (Fig. 6G-H). Again, within the first 10 fractions (fraction 10 to 20), the molarity of the product Lewis^X-*t*Boc reaches a maximum of approximately 3.5 mM and is declining sharply in the later fractions representing the combined reaction/diafiltration mode. Interestingly, after a delay of around one hour the concentration of the acceptor sugar LacNAc-*t*Boc also starts to rise and reaches a molarity between 3 and 4 mM until the end of period c (see Fig. 6G). Same as for LacNAc-*t*Boc synthesis, the nucleotide sugar increases up to 3.5 mM in period b, followed by a sharp decrease at the beginning of period c, which is then interrupted by a temporary peak, assumingly caused by a change in membrane retention. By the start of diafiltration (fraction 20) also the concentration degradation product guanosine is reduced to very low levels (<0.5 mM) (Fig. 6H).

In summary, the conversions achieved in the initial pure reaction mode again are consistent with the activity levels determined in standard batch assays when interpreted with a simplified PFR framework. Using $\tau \approx 60$ min and $a_V = k \bullet C_{in}$ with $k = -\tau^{-1}\ln\left(\frac{C_{out}}{C_{in}}\right)$, the maximum LacNAc-*t*Boc concentrations of ~3.5 mM obtained from a 5 mM GlcNAc-*t*Boc feed (i.e., $\frac{C_{out}}{C_{in}} \approx 0.30$) correspond to $k \approx 0.020$ min^{-1} and an effective volumetric activity of $a_V \approx 0.10$ U mL$^{-1} \approx 100$ mU mL^{-1} for the SpyC-β4GalT microgel step. This value is in the same order as the standard assay activity of the corresponding carrier (132 mU mL^{-1}, Table S7), despite the fact that the assay was performed under enzyme-optimal conditions (notably at alkaline pH), whereas the reactor was operated under a pH compromise required for sequential processing. Analogously, the maximum Lewis^X-*t*Boc concentrations of ~3.5 mM from a 5 mM LacNAc-*t*Boc feed imply a V ≈ 100 mU mL^{-1} for the fucosylation step, which compares well to the standard assay activity of the SpyT-agarose carrier (120 mU mL^{-1}, Table S7). The close agreement for immobilized SpyC-α3,4FucT is plausible given the smaller deviation between assay and reactor conditions, and it further suggests that the reactions may not operate fully in the strictly linear substrate-limited regime (e.g., due to relatively low apparent K_M values for the respective acceptors). In the subsequent combined reaction/diafiltration mode, the pronounced decrease of outlet concentrations should therefore not be interpreted primarily as a loss of catalytic activity, but rather as an apparent effect caused by system hydrodynamics and membrane-mediated redistribution/permeation.

3.3.3. Synthesis of Galili-tBoc

While the individual reactor modules offer the benefit of a modular combination of different immobilized enzymes in distinct modules and precise monitoring of intermediates, the following approaches are based on the combination of different enzymes in one reactor module. A combination of multiple immobilized enzymes in one reactor allows a faster product recovery and simplified reaction set-up. On the other hand, this strategy harbors various challenges, including a limited reactor volume and the need for a sophisticated adjustment of reactor conditions in order to achieve satisfying conversion rates for all involved enzymes. Therefore, for the following syntheses, different strategies for each approach were investigated.

First, the Galili-*t*Boc was synthesized starting from GlcNAc-*t*Boc, to synthesize the intermediate LacNAc-*t*Boc by addition of a galactose glycone from UDP-Gal with the help of immobilized SpyC-β4GalT, and finally the final product Galili-*t*Boc by addition of another galactose from UDP-Gal. Noteworthy, the synthesis of the Galili-*t*Boc followed two strategies. First, microgels with immobilized SpyC-β4GalT and SpyC-

α3GalT were embedded in the same reactor module, resulting in the reduction of the total enzyme amount due to the shared limited reaction environment size (Fig. 7A). Secondly, to increase the space for the individual enzymes, a precolumn with SpyC-β4GalT immobilized on Ni^{2+}-IDA beads was installed for the synthesis of LacNAc-*t*Boc, which was directly transferred to the reactor module, harboring the microgel immobilized SpyC-α3GalT (Fig. 7B). Both strategies applied a sequential reaction mode in the used double-membrane reaction module, starting with plain reaction mode (fractions 10–21) followed by a combined reaction/diafiltration (fractions 22–35). To this end, individual fractions of both runs were collected, and the glycan yield was analyzed. The synthesis of the Galili-*t*Boc using free or microgel-immobilized enzymes in one-pot reactions was demonstrated before [7].

To monitor the enzymatic conversion of the substrate GlcNAc-*t*Boc to the intermediate LacNAc-*t*Boc and the final product Galili-*t*Boc, the glycan yield of individual reactor fractions was measured by HPLC-UV analysis (Fig. 7C, Fig. S11). Applying the first strategy with the mixture of microgels in the same reactor module yielded up to 32% for the intermediate LacNAc-*t*Boc at the end of the pure reaction period (fraction 19). When switching to the reaction/diafiltration mode the conversion rate dropped to around 20% for the reasons described in the previous chapter. Furthermore, the yield of the final product Galili-*t*Boc was negligible in both periods.

As described, in this first strategy both carriers were co-packed in a single 0.6 mL reactor chamber, such that only ~300 µL reactor volume was available per immobilized enzyme. Even during the period of pure reaction mode, the first step (GlcNAc-*t*Boc → LacNAc-*t*Boc) reached only ~30% conversion at 1 mM GlcNAc-*t*Boc and 2.6 mM UDP-Gal in the feed, which, under the assumption of strictly substrate limited kinetics for both GlcNAc-*t*Boc and UDP-Gal, corresponds with a required specific activity of the β4GalT microgel of around 60 mU mL^{-1}. This is markedly below the standard assay activity of the corresponding SpyC-β4GalT microgel (234 mU mL^{-1}), but becomes plausible when accounting for the strongly reduced substrate levels applied in the reactor experiment relative to the assay (1 mM/2.6 mM vs. 5 mM/6.5 mM). Assuming substrate limited kinetics for the donor and the acceptor, this gives a factor of (1/5)·(2.6/6.5) ≈ 0.08, corresponding to a worst-case estimation of ~19 mU mL^{-1} for the specific activity. The comparison gives a reasonable explanation of the low LacNAc-*t*Boc yield despite the relatively high activity the SpyC-β4GalT microgel showed in the standard assay. In addition, it also shows that the assumption of a multiplicative effect of substrate limitation of the acceptor and donor species is a worst-case scenario, which is not fully applicable in the used concentration range. Nevertheless, for the second step (LacNAc-*t*Boc ➔ Galili-*t*Boc), Galili formation is negligible, which is consistent with the very low effective driving force for this α3GalT catalyzed reaction. First, the acceptor LacNAc-*t*Boc is generated in situ and is present only at sub-millimolar levels, and second the SpyC-α3GalT microgel exhibits a substantially lower standard assay activity (39 mU mL^{-1}) than immobilized SpyC-β4GalT. After scaling for the reduced acceptor and donor concentrations, the estimated effective specific activity falls in the range of only 1 mU mL^{-1}, so that near-zero Galili formation is the anticipated outcome. Noteworthy, the synthesis of the Galili epitope by microgel immobilized SpyC-β4GalT and SpyC-α3GalT was achieved before [7]. However, the incubation time in this this previous study was up to 100 h in a one-pot cascade. Therefore, the possibility of this reaction was demonstrated, however, limitations in enzyme volume and reaction time hamper the efficiency in a reactor environment.

Therefore, separating immobilized SpyC-β4GalT and SpyC-α3GalT into a high-activity precolumn followed by a dedicated reactor module for the second reaction step fundamentally changed the kinetic situation compared to the first strategy. In the precolumn, only SpyC-β4GalT immobilized on Ni^{2+}–IDA carriers, was employed. Although no standard assay activity was determined for this specific carrier batch, earlier work with Ni^{2+}-IDA-bound SpyC-β4GalT consistently demonstrated high enzyme loadings (92.7%, Table S4) and, under near-saturating substrate conditions, volumetric activities exceeding 600 mU mL^{-1} [18]. On this basis, quantitative conversion of GlcNAc-*t*Boc to LacNAc-*t*Boc in the precolumn was expected and was experimentally confirmed, effectively delivering ~1 mM LacNAc-*t*Boc to the downstream reactor. At the same time, near-complete turnover of 1 mM acceptor in the precolumn implies consumption of approximately 1 mM UDP-Gal, leaving ~1.6 mM

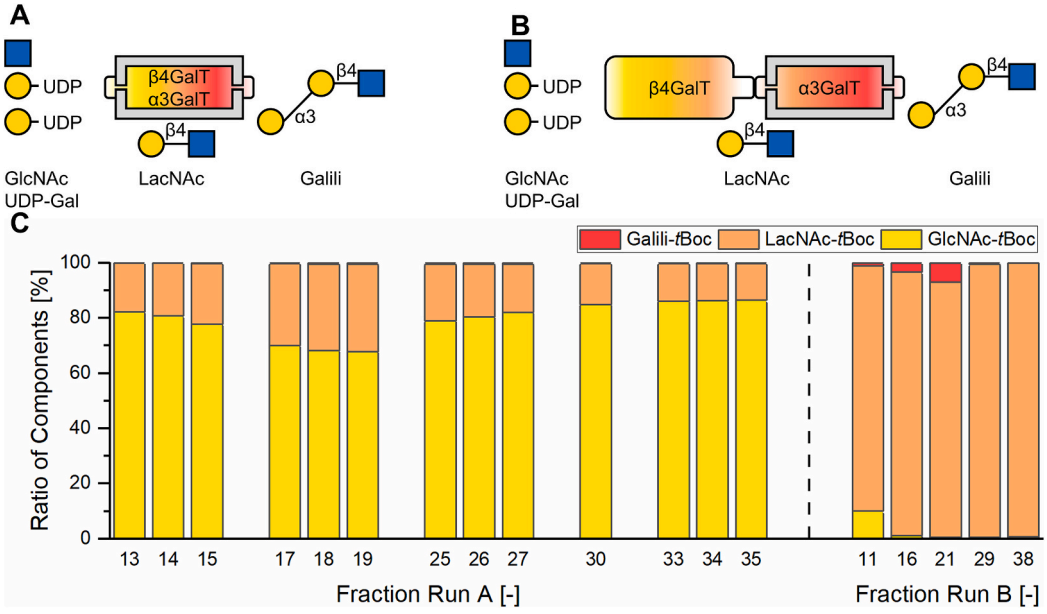

Fig. 7. Synthesis of Galili-*t*Boc with two different reactor strategies. A) The reaction mix containing UDP-Gal and GlcNAc-*t*Boc is transferred through the reaction chamber of the reactor module, containing microgel immobilized SpyC-β4GalT and SpyC-α3GalT. The intermediate LacNAc-*t*Boc is produced within the same reactor module. B) An identical reaction mix is used, and synthesis of LacNAc-*t*Boc with Ni^{2+}-IDA immobilized SpyC-β4GalT is performed in a precolumn. The second reaction step for the formation of the Galili-*t*Boc is performed in the reactor module with microgel immobilized SpyC-α3GalT. C) Glycan yield for reactor synthesis of the Galili-tBoc in a single reactor module (Run A) and precolumn approach (Run B). The percentage yield of the precursor GlcNAc-tBoc, the intermediate LacNAc-tBoc, and the final product Galili-*t*Boc in individually selected fractions, analyzed by HPLC-UV, are shown.

UDP-Gal available for the subsequent SpyC-α3GalT-catalyzed step. The strongly increased LacNAc-*t*Boc concentration in combination with doubling the amount of applied SpyC-α3GalT microgel in the dedicated reactor module made it possible to achieve a Galili yield of up to 7% in the pure reaction mode (period b) despite the low intrinsic activity of the SpyC-α3GalT microgel (standard assay activity ~39 mU mL^{-1}). In summary, strategy 2 (Fig. 7B) demonstrates that achieving quantitative formation of the intermediate is feasible by decoupling the first step into a highly active SpyC-β4GalT precolumn, while the overall yield remains limited by the low effective activity of the downstream SpyC-α3GalT step. However, increasing the residence time in the second step and/or improving the enzyme loading of the SpyC-α3GalT microgel are clear approaches to achieving high yields for Galili synthesis in a multi-stage, continuous reactor system.

3.3.4. *Synthesis of blood group A tetraose type VI*

Reaction (iv) serves as a proof-of-concept for executing a two-enzyme glycan synthesis in a single EMR module using a mixed carrier bed. In contrast to the one-module Galili cascade in reaction (iii), which did not yield appreciable final product due to an unfavorable balance between intermediate formation and consumption, the blood group A (BGA) tetraose type VI synthesis was selected to demonstrate that in situ generation and subsequent turnover of an intermediate can be realized within one reactor chamber. Here, a α2FucT (FutC) was used for the synthesis of the intermediate 2′-fucosyllactose (2′-FL, H-antigen type VI). While the activity of the enzyme is rather low, immobilization in microgels and SpyT-agarose further reduces the activity to a negligible point [8]. Therefore, for this approach, Ni^{2+}-IDA beads were utilized to immobilize α2FucT (Fig. 8A). For the subsequent synthesis of BGA from 2′-FL, immobilized SpyC-GTA was used. Therefore, Ni^{2+}-IDA immobilized SpyC-GTA and FutC were embedded into the reactor for synthesis of the final product BGA from lactose. The yield of substrate, intermediate and product glycans were analyzed via xCGE-LIF (Fig. 8B, Fig. S13). Additionally, SpyC-GTA was immobilized on microgels and utilized for synthesis of BGA (Fig. S6).

In this combinatory approach of α2FucT and SpyC-GTA on Ni^{2+}-IDA for BGA synthesis from lactose approximately 7% final product on average through all fractions was achieved, while the remaining glycans represent the precursor lactose (Fig. 8B). Noteworthy, with applying the crossflow (represented after fraction 20 and 21, Fig. 9B) the proportion of the final product among the detected saccharides increased from 5.9% to 8.8%, corresponding to a relative increase of approximately 49%. No intermediate 2′-FL was detected in any fraction. Given the comparatively high activity of SpyC-GTA relative to α2FucT, the intermediate is rapidly converted into the final product, resulting in no detectable accumulation of the intermediate glycan. Immobilization of SpyC-GTA on microgels instead of Ni^{2+}-IDA beads results in a decreased enzymatic activity and therefore slight accumulation of the intermediate 2′-FL (Fig. S6). However, applying this less active immobilized enzyme drastically results the final BGA yield to only 2–3% (Fig. S6). In both cases, the precursor lactose represents the major glycan fraction.

3.3.5. *Strategies towards a continuous flow reactor*

To overcome the limited conversion rates observed in the current enzymatic membrane flow reactor, a combination of different engineering and biocatalyst-related modifications can be pursued rather than relying on a single change. First, the effective catalytic capacity inside the reactor can be increased by raising the enzyme loading and by reducing the flow rates to provide longer residence times. This would allow substrates to spend more time in contact with the catalytic material and partially compensate for the low specific activity of the currently used glycosyltransferases. Since the low intrinsic activity of the immobilized enzymes is a major contributor to the limited conversion, an obvious complementary strategy is the selection or development of more active biocatalysts. Alternative enzymes with higher turnover numbers, even if they are somewhat less selective, could be evaluated to identify a suitable compromise between activity and selectivity under the chosen reaction conditions. In the longer term, protein engineering approaches such as directed evolution could be applied to generate glycosyltransferase variants with improved catalytic efficiency and stability under the operating conditions of the membrane reactor, thereby directly addressing the enzymatic bottleneck.

For larger glycans, the use of membranes with a higher MWCO may simplify the separation of smaller by-products; however, these membranes were not suitable for investigation in the present study because of the lower molecular weight of the target compounds. In the case of BGA, for example, such membranes could potentially have allowed the separation of a larger proportion of lactose from the reaction mixture.

In addition to these biocatalyst-focused strategies, the hydrodynamics of the diafiltration operation need to be optimized. Upon initiation of the diafiltration stream, we observed a pronounced drop in conversion, which can be attributed to the accumulation of substrate at the membrane surface while the immobilized enzyme remains confined to the structure of the middle compartment due to the carrier remaining there. This spatial separation reduces substrate–enzyme contact and thus suppresses reaction turnover. One possible way to mitigate this

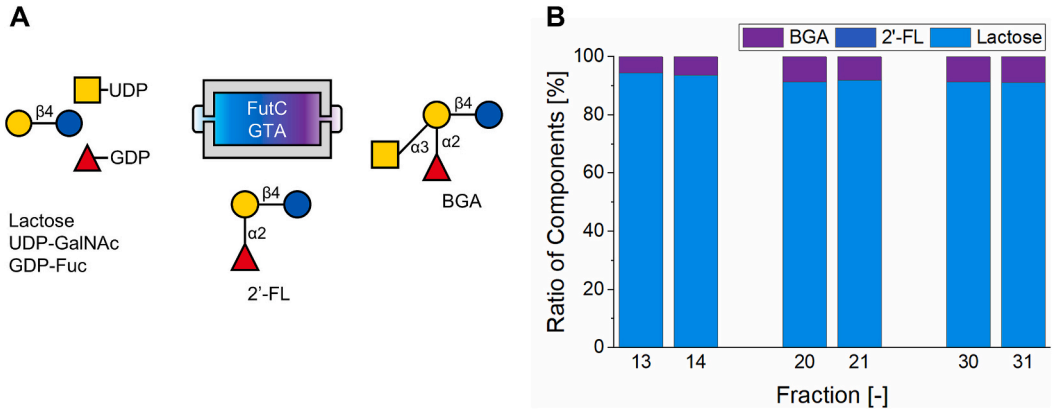

Fig. 8. Synthesis of blood group A tetraose type VI in the reactor module. A) A reaction mix containing lactose, UDP-GalNAc, and GDP-Fuc flows through the reactor containing the enzymes FutC and SpyC-GTA. FutC is immobilized in Ni^{2+}-IDA beads. SpyC-GTA is either immobilized on Ni^{2+}-IDA beads in a first approach or on microgels in the second approach. Syntheses of the intermediate, 2′-fucosyllactose, as well as the final product, blood group A tetraose type VI, both take place within the same reactor module. B) Glycan Yield for reactor synthesis of the blood group A tetraose type VI epitope (BGA). FutC and SpyC-GTA were immobilized on Ni^{2+}-IDA beads. Percentage yield of the precursor lactose, the intermediate 2′-fucosyllactose (2′-FL), and the final product blood group A tetraose (all determined via xCGE-LIF) in individually selected fractions are shown.

effect is to modulate the diafiltration flow rate in a time-dependent manner, for instance by alternating the inlet between the upper and lower compartments, as was demonstrated when performing ultrafiltration in a similar module [41]. This is expected to enhance mixing in the middle compartment and restore contact between substrate and catalyst, thereby increasing conversion rates.

4. Conclusion

In this work, we successfully established a modular continuous flow reactor for automated enzymatic glycan synthesis. The reactor design enables precise control of flow rates and selective removal of by-products, while products and immobilized enzymes are retained in the reaction chamber. Through the modular combination of individual enzyme reactors in a sequential synthesis, defined glycan structures could be produced efficiently, resulting in yields of 36% for LNFPIII and 30% for Lewis^X. In contrast, cascading several enzymes within a single reactor ("one-pot approach") resulted in significantly lower yields of a maximum of 7% for both, Galili-*t*Boc and BGA, respectively, reflecting the current limitations of the system in terms of synthesis rates, enzyme activity, and limited reaction volume. The technical challenges and corresponding solutions were discussed in detail. Importantly, the system is not only capable for one limited immobilization technique, but rather different techniques, namely microgels, SpyT-agarose and commercial Ni^{2+}-IDA beads were applied. This offers the possibility to carefully select the preferred immobilization strategy for embedment in the reactor module.

Despite incomplete conversion, the initial results clearly demonstrate the potential of the reactor system. Scaling up the reactor volume to increase enzyme loading, optimizing the flow rate, and extending the residence time offer concrete starting points for increasing productivity rates. Since many glycosyltransferases have low turnover rates, the platform also opens up the possibility of achieving higher conversion rates for alternative products through replacement or combination with more active enzyme classes. Another promising approach is the reuse of reactor modules over several synthesis cycles, as already described for immobilized enzymes [8]. Overall, MiRAGE should be regarded as a modular prototype platform for automated multistep glycan synthesis and in situ process conditioning, rather than as a fully optimized preparative production system. The present results demonstrate the versatility of the reactor concept and provide a foundation for further development towards more robust and productive AEGS platforms.

Future perspective of this platform offers substantial potential for development and optimization. Expansion of the repertoire of immobilized glycosyltransferases enable the synthesis of various, more complex glycans. The potential formation of byproducts of other glycans in the syntheses of longer glycans is an important consideration. However, glycosyltransferases are generally characterized by a high degree of regio- and stereoselectivity, which reduces the formation of undesired products in comparison to conventional chemical strategies. Previous studies employing free and immobilized glycosyltransferases, used in this study, have already demonstrated the efficiency of structurally complex glycans using free or immobilized enzymes [8,53]. Therefore, transferring such enzymatic cascades to the reactor system presents an expansion of these earlier findings. Moreover, other research groups installed enzyme assembly synthetic maps or intermediate enzymatic modification steps to guide one-pot stepwise synthesis of complex HMOs with glycosyltransferases [54,55]. These strategies may also be transferred to our described reactor concept. Consequently, while increasing glycan length may increase reaction complexity, the inherent selectivity of the enzymes is expected to limit unwanted byproduct formation and thereby maintain the practicability of the approach.

Previous work already demonstrated the successful immobilization of further enzymes, applicable for further implementation [7,8,56]. Moreover, the reusability of reactor embedded enzymes represents a promising value to improve both, sustainability and process efficiency. This may be achieved through storage and repeated deployment of the reactor-enzyme modules, as well as through strategic adjustments to reactor operation as a retention stream for repeated reaction flow through the reactor module to increase total residence time. An increase in residence time could also be achieved by adjustments of flow rate or reaction chamber volume. Finally, the MiRAGE platform was demonstrated to be functional with immobilized glycosyltransferases. As the inherent enzymatic activity of glycosyltransferases is rather low, the overall functional reactor could be applied for incorporation of alternative enzymes with complementary activities and thus could drastically enhance the substrate turnover productivity and therefore, demonstrate the versatility of the system.

Most recent examples for automated enzymatic glycan synthesis include different reactor concepts are described in our latest review on automated enzymatic glycan synthesis [2]. Early proof-of-concept studies demonstrated that enzymatic oligosaccharide synthesis can be implemented on commercially available peptide synthesizers by adapting solid-phase workflows and thermoresponsive supports [16]. Here, using multiple enzymes, yields between 9 and 38% have been achieved for several important oligosaccharides. In another study, automated chemoenzymatic modular synthesis of LNFPIII in a microfluidic and bead-based system enabling multi step glycan assembly resulted in yield of 71% [57]. However, in contrast to automated peptide or nucleic acid synthesis, current enzymatic glycan synthesis platforms remain less standardized and are often limited in scalability, glycan yields or diversity, as well as downstream processing. Chakraborty and colleagues developed an automated chemoenzymatic synthesis platform based on a "catch-and-release" strategy, where glycosyltransferase-catalyzed reactions are performed in solutions and intermediates are purified via solid-phase extraction [58]. The workflow was fully automated using an AI Swing Isynth (Chemspeed) system, enabling precise reaction mixture handling. Importantly, the capture process involved two columns, Ni^{2+}-IDA for capture of the His-tagged enzymes and a C18 resin for capture of the glycan products. This design enables streamlined, reproducible synthesis with minimal manual intervention. To achieve targeted N-glycosylation, another study introduces a modular glycoengineering platform that employs immobilized enzymes to enable sequential, pathway-like reactions mimicking Golgi reaction processing [59]. Immobilized enzymes allow their reuse and assembly into a controlled cascade for stepwise glycosylation. The system achieves high control of glycoformes, for example reaching to 80–96% terminal glycosylation. Enzyme recyclability over extended reaction times above 80 h highlight its efficiency, scalability and suitability for producing of well-defined glycans.

While yields obtained with the current MiRAGE platform remained below those reported for more advanced automated glycan synthesis systems, the intrinsic concept of combining modular glycan synthesis with membrane cross-flow was to integrate product formation with in situ process conditioning. In this context, MiRAGE represents a significant step towards automated enzymatic glycan synthesis by enabling sequential reactor operation, online monitoring of reactor parameters, buffer exchange between reaction steps, and partial removal of low-molecular-weight side components via cross-flow membrane operation. Furthermore, we demonstrated the versatility of enzyme implementation via different immobilization and embedment strategies. Thereby, different key bottlenecks that have so far hindered the widespread adoption of automatic enzymatic glycan synthesis have been addressed.

Author disclosure

K.P.H., L.E. and M.F. designed this study. K.P.H. and P.P. designed and expressed the SpyC-GT constructs. P.P. and M.I.P. immobilized the SpyC-GTs in agarose and microgels, respectively. M.I.P. characterized the microgels. U.T. and K.B. designed the bioreactor. K.P.H., M.I.P., U.T. and P.P. performed the reactor runs. K.P.H., P.P., R.B., and R.H.

performed the glycan and co-factor analyses. K.P.H., M.I.P., and U.T. wrote the manuscript and designed the figures. A.P., M.F., E.R., and L.E. proposed the project conceptualization. All authors contributed to the discussion, editing, and completion of the manuscript, and all authors approved the final submitted version.

CRediT authorship contribution statement

Kai P. Hussnaetter: Writing – review & editing, Writing – original draft, Visualization, Supervision, Project administration, Methodology, Investigation, Formal analysis, Data curation, Conceptualization. **Maria I. Pieper:** Writing – review & editing, Writing – original draft, Visualization, Validation, Investigation, Formal analysis, Data curation. **Ulrich Thiele:** Writing – review & editing, Writing – original draft, Visualization, Validation, Methodology, Investigation, Formal analysis, Data curation. **Philip Palm:** Writing – review & editing, Methodology, Investigation. **Robert Burock:** Writing – review & editing, Writing – original draft, Methodology, Investigation. **René Hennig:** Writing – review & editing, Methodology, Investigation. **Katharina Bleher:** Writing – review & editing, Methodology, Investigation. **Andrij Pich:** Writing – review & editing, Supervision, Resources, Project administration, Funding acquisition, Conceptualization. **Matthias Franzreb:** Writing – review & editing, Writing – original draft, Supervision, Resources, Project administration, Funding acquisition, Conceptualization. **Erdmann Rapp:** Writing – review & editing, Supervision, Resources, Project administration, Funding acquisition, Conceptualization. **Lothar Elling:** Writing – review & editing, Writing – original draft, Supervision, Resources, Project administration, Funding acquisition, Conceptualization.

Funding

We gratefully acknowledge financial support from the Federal Ministry of Research, Technology and Space (BMFTR) through the project “MiRAGE: Microgel continuous flow reactor for automated glycan synthesis with immobilized enzymes” (AZ: 031B1116A-D) as part of the BMFTR program Future technologies for the industrial bioeconomy: focus on biohybrid technologies.

Declaration of competing interest

ER is the founder of glyXera GmbH. RH is co-founder and CSO of glyXera GmbH. RB was an employee of glyXera GmbH. glyXera provides high-performance glycoanalytical products and services, and holds several patents for xCGE-LIF-based glycoanalysis. All other authors declare that they have no known competing financial interests or personal relationships that could have appeared to influence the work reported in this paper. There are no additional relationships or activities, or patents to disclose.

Acknowledgments

The authors thank Prof. Ing. Vladimír Křen, PhD., DSc., FRSC, and Prof. RNDr. Pavla Bojarová, Ph.D. (Laboratory of Biotransformation at the Institute of Microbiology of the Czech Academy of Sciences, Prague) for providing *t*Boc-linked sugars. Additionally, we are grateful to Isabelle Zupanc for support with microgel synthesis and characterization, and to Shannon Anna Jung for nanoindentation measurements. Thanks to Truc Pham for help with enzyme purification and to Dennis Hirtz for support with analytical methods.

Appendix A. Supplementary data

Supplementary data to this article can be found online at https://doi.org/10.1016/j.cej.2026.178229.

Data availability

Data will be made available on request.

References

[1] B. Nidetzky, A. Gutmann, C. Zhong, Leloir glycosyltransferases as biocatalysts for chemical production, ACS Catal. 8 (2018) 6283–6300, https://doi.org/10.1021/acscatal.8b00710.
[2] K.P. Hussnaetter, P. Palm, A. Pich, M. Franzreb, E. Rapp, L. Elling, Strategies for automated enzymatic glycan synthesis (AEGS), Biotechnol. Adv. 67 (2023) 108208, https://doi.org/10.1016/j.biotechadv.2023.108208.
[3] T. Man, C. Xu, X.-Y. Liu, D. Li, C.-K. Tsung, H. Pei, Y. Wan, L. Li, Hierarchically encapsulating enzymes with multi-shelled metal-organic frameworks for tandem biocatalytic reactions, Nat. Commun. 13 (2022) 305, https://doi.org/10.1038/s41467-022-27983-9.
[4] W. Gao, S. Shi, Y. Li, F. Liu, Y. Cheng, J. Zheng, M. Qiao, S. Yuan, X. Zhang, DNA-directed assembly of core-satellite MOF structures for spatially compartmentalized multi-enzyme cascade catalysis, Chem. Eng. J. 529 (2026) 173137, https://doi.org/10.1016/j.cej.2026.173137.
[5] Y. Li, X. Xu, B. Yan, C. Deng, W. Yu, P. Yang, X. Zhang, Microchip reactor packed with metal-ion chelated magnetic silica microspheres for highly efficient proteolysis, J. Proteome Res. 6 (6) (2007) 2367–2375, https://doi.org/10.1021/pr060558r.
[6] M. Baeza, C. López, J. Alonso, J. López-Santín, G. Álvaro, Ceramic microsystem incorporating a microreactor with immobilized biocatalyst for enzymatic spectrophotometric assays, Anal. Chem. 82 (3) (2010) 1006–1011, https://doi.org/10.1021/ac902267f.
[7] I.K. Sommerfeld, P. Palm, K.P. Hussnaetter, M.I. Pieper, S. Bulut, T. Lile, R. Wagner, J.J. Walkowiak, L. Elling, A. Pich, Microgels with immobilized glycosyltransferases for enzymatic glycan synthesis, Biomacromolecules 25 (2024) 3807–3822, https://doi.org/10.1021/acs.biomac.4c00409.
[8] P. Palm, K.P. Hussnaetter, L. Elling, Glycan synthesis with SpyCatcher-SpyTag immobilized Leloir-glycosyltransferases, Appl. Microbiol. Biotechnol. 109 (2025) 234, https://doi.org/10.1007/s00253-025-13602-2.
[9] M. Qiao, Y. Ji, R.J. Linhardt, X. Zhang, H. Huang, Fabricating bimetal organic material capsules with a commodious microenvironment and synergistic effect for glycosyltransferase, ACS Appl. Mater. Interfaces 14 (22) (2022) 26034–26043, https://doi.org/10.1021/acsami.2c04644.
[10] F. Lackner, H. Liu, A.D. Štiglic, M. Bračič, R. Kargl, B. Nidetzky, T. Mohan, K. S. Kleinschek, 3D printed porous Nanocellulose-based scaffolds as carriers for immobilization of glycosyltransferases, ACS Appl. Bio Mater. 5 (12) (2022) 5728–5740, https://doi.org/10.1021/acsabm.2c00763.
[11] H. Liu, B. Nidetzky, Leloir glycosyltransferases enabled to flow synthesis: continuous production of the natural C-glycoside nothofagin, Biotechnol. Bioeng. 118 (11) (2021) 4402–4413, https://doi.org/10.1002/bit.27908.
[12] Z. Su, J. Luo, X. Li, M. Pinelo, Enzyme membrane reactors for production of oligosaccharides: a review on the interdependence between enzyme reaction and membrane separation, Sep. Purif. Technol. 243 (2020) 116840, https://doi.org/10.1016/j.seppur.2020.116840.
[13] L. Giorno, E. Drioli, Biocatalytic membrane reactors: applications and perspectives, Trends Biotechnol. 18 (2000) 339–349, https://doi.org/10.1016/S0167-7799(00)01472-4.
[14] V. Calabrò (Ed.), Engineering Aspects of Membrane Bioreactors, Woodhead Publishing / Elsevier, 2013.
[15] L. Hilterhaus, A. Liese (Eds.), Applications of Reaction Engineering to Industrial Biotransformations, Wiley, 2009.
[16] J. Zhang, C. Chen, M.R. Gadi, C. Gibbons, Y. Guo, X. Cao, G. Edmunds, S. Wang, D. Liu, J. Yu, L. Wen, P.G. Wang, Machine-driven enzymatic oligosaccharide synthesis by using a peptide synthesizer, Angew. Chem. Int. Ed. 57 (2018) 16638–16642, https://doi.org/10.1002/anie.201810661.
[17] R. Heinzler, J. Hübner, T. Fischöder, L. Elling, M. Franzreb, A compartmented flow microreactor system for automated optimization of bioprocesses applying immobilized enzymes, Front. Bioeng. Biotechnol. 6 (2018) 189, https://doi.org/10.3389/fbioe.2018.00189.
[18] R. Heinzler, T. Fischöder, L. Elling, M. Franzreb, Toward automated enzymatic glycan synthesis in a compartmented flow microreactor system, Adv. Synth. Catal. 361 (2019) 4506–4516, https://doi.org/10.1002/adsc.201900709.
[19] R. Greifenstein, T. Ballweg, T. Hashem, E. Gottwald, D. Achauer, F. Kirschhöfer, M. Nusser, G. Brenner-Weiß, E. Sedghamiz, W. Wenzel, E. Mittmann, K.S. Rabe, C. M. Niemeyer, M. Franzreb, C. Wöll, MOF-hosted enzymes for continuous flow catalysis in aqueous and organic solvents, Angew. Chem. Int. Ed. 61 (18) (2022) e202117144, https://doi.org/10.1002/anie.202117144.
[20] Q. Sun, B. Aguila, P.C. Lan, S. Ma, Tuning pore heterogeneity in covalent organic frameworks for enhanced enzyme accessibility and resistance against denaturants, Adv. Mater. 31 (19) (2019) 1900008, https://doi.org/10.1002/adma.201900008.
[21] B. Schmieg, J. Döbber, F. Kirschhöfer, M. Pohl, M. Franzreb, Advantages of hydrogel-based 3D-printed enzyme reactors and their limitations for biocatalysis, Front. Bioeng. Biotechnol. 6 (2018) 211, https://doi.org/10.3389/fbioe.2018.00211.
[22] G. Chen, X. Kou, S. Huang, L. Tong, Y. Shen, W. Zhu, F. Zhu, G. Ouyang, Modulating the biofunctionality of metal–organic-framework-encapsulated enzymes through controllable embedding patterns, Angew. Chem. Int. Ed. 59 (7) (2020) 2867–2874, https://doi.org/10.1002/anie.201913231.

[23] N. Welsch, A. Wittemann, M. Ballauff, Enhanced activity of enzymes immobilized in Thermoresponsive Core−Shell microgels, J. Phys. Chem. B 113 (49) (2009) 16039–16045, https://doi.org/10.1021/jp907508w.
[24] A. Biffis, L. Minati, Efficient aerobic oxidation of alcohols in water catalysed by microgel-stabilised metal nanoclusters, J. Catal. 236 (2) (2005) 405–409, https://doi.org/10.1016/j.jcat.2005.10.012.
[25] X. Liu, J. Yang, L. Yang, Capillary electrophoresis-integrated immobilized enzyme reactors, Rev. Anal. Chem. 35 (2016) 115–131, https://doi.org/10.1515/revac-2016-0003.
[26] A.H. Keeble, P. Turkki, S. Stokes, I.N.A. Khairil Anuar, R. Rahikainen, V. P. Hytönen, M. Howarth, Approaching infinite affinity through engineering of peptide-protein interaction, Proc. Natl. Acad. Sci. USA 116 (2019) 26523–26533, https://doi.org/10.1073/pnas.1909653116.
[27] A.H. Keeble, M. Howarth, Insider information on successful covalent protein coupling with help from SpyBank, Methods Enzymol. 617 (2019) 443–461, https://doi.org/10.1016/bs.mie.2018.12.010.
[28] B. Sauerzapfe, D.-J. Namdjou, T. Schumacher, N. Linden, K. Křenek, V. Křen, L. Elling, Characterization of recombinant fusion constructs of human β1,4-galactosyltransferase 1 and the lipase pre-propeptide from staphylococcus hyicus, J. Mol. Catal. B Enzym. 50 (2008) 128–140, https://doi.org/10.1016/j.molcatb.2007.09.009.
[29] B. Sauerzapfe, K. Krenek, J. Schmiedel, W.W. Wakarchuk, H. Pelantová, V. Kren, L. Elling, Chemo-enzymatic synthesis of poly-N-acetyllactosamine (poly-LacNAc) structures and their characterization for CGL2-galectin-mediated binding of ECM glycoproteins to biomaterial surfaces, Glycoconj. J. 26 (2009) 141–159, https://doi.org/10.1007/s10719-008-9172-2.
[30] V. Heine, H. Pelantová, P. Bojarová, V. Křen, L. Elling, Targeted Fucosylation of Glycans with engineered bacterial Fucosyltransferase variants, ChemCatChem 14 (2022) e202200037, https://doi.org/10.1002/cctc.202200037.
[31] N.O. Seto, M.M. Palcic, C.A. Compston, H. Li, D.R. Bundle, S.A. Narang, Sequential interchange of four amino acids from blood group B to blood group a glycosyltransferase boosts catalytic activity and progressively modifies substrate recognition in human recombinant enzymes, J. Biol. Chem. 272 (1997) 14133–14138, https://doi.org/10.1074/jbc.272.22.14133.
[32] G. Wang, D.A. Rasko, R. Sherburne, D.E. Taylor, Molecular genetic basis for the variable expression of Lewis Y antigen in helicobacter pylori: analysis of the alpha (1,2) fucosyltransferase gene, Mol. Microbiol. 31 (1999) 1265–1274, https://doi.org/10.1046/j.1365-2958.1999.01268.x.
[33] T. Fischöder, D. Laaf, C. Dey, L. Elling, Enzymatic synthesis of N-Acetyllactosamine (LacNAc) type 1 oligomers and characterization as multivalent galectin ligands, Molecules 22 (2017), https://doi.org/10.3390/molecules22081320.
[34] S. Bulut, D. Günther, M. Bund, C. Haats, T. Bissing, C. Bastard, M. Wessling, L. de Laporte, A. Pich, Cellular architects at work: cells building their own microgel houses, Adv. Healthc. Mater. 13 (2024) e2302957, https://doi.org/10.1002/adhm.202302957.
[35] D. Rommel, B. Häßel, P. Pietryszek, M. Mork, O. Jung, M. Emondts, N. Norkin, I. C. Doolaar, Y. Kittel, G. Yazdani, A. Omidinia-Anarkoli, S. Schweizerhof, K. Kim, A. Mourran, M. Möller, J. Guck, L. de Laporte, Thermally assisted microfluidics to produce chemically equivalent microgels with tunable network morphologies, Angew. Chem. Int. Ed. 64 (2025) e202411772, https://doi.org/10.1002/anie.202411772.
[36] B. González-Bermúdez, G.V. Guinea, G.R. Plaza, Advances in micropipette aspiration: applications in cell biomechanics, models, and extended studies, Biophys. J. 116 (2019) 587–594, https://doi.org/10.1016/j.bpj.2019.01.004.
[37] A.A. Moud, Fluorescence recovery after Photobleaching in colloidal science: introduction and application, ACS Biomater Sci. Eng. 8 (2022) 1028–1048, https://doi.org/10.1021/acsbiomaterials.1c01422.
[38] D.M. Soumpasis, Theoretical analysis of fluorescence photobleaching recovery experiments, Biophys. J. 41 (1983) 95–97, https://doi.org/10.1016/S0006-3495(83)84410-5.
[39] H.W. Ooi, H. Peng, K.S. Jack, A.K. Whittaker, Understanding the diffusion of Dextrans in 'click' PNIPAAm hydrogels, Aust. J. Chem. 67 (2014) 85–92, https://doi.org/10.1071/CH13333.
[40] B. Zakeri, J.O. Fierer, E. Celik, E.C. Chittock, U. Schwarz-Linek, V.T. Moy, M. Howarth, Peptide tag forming a rapid covalent bond to a protein, through engineering a bacterial adhesin, Proc. Natl. Acad. Sci. USA 109 (2012) E690–E697, https://doi.org/10.1073/pnas.1115485109.
[41] R. Tan, F. Hezel, M. Franzreb, Continuous single pass diafiltration with alternating permeate flow direction for high efficiency buffer exchange, J. Membr. Sci. 619 (2021) 118695, https://doi.org/10.1016/j.memsci.2020.118695.
[42] U. Thiele, T. Kaloghlian, J. Wohlgemuth, G. Brenner-Weiß, A. Tschöpe, M. Franzreb, K. Bleher, Fractionation of oligosaccharide nucleoside mixtures by single pass Nano-Diafiltration, Eng. Life Sci. 25 (2025) e70055, https://doi.org/10.1002/elsc.70055.
[43] A.H. Hellinga, S. Cajic, H.F. Linde, A.H. van Stigt, J.H.M. de Vries, E.M. Brouwer-Brolsma, R. Hennig, E. Rapp, M. Mank, B. Stahl, A.D. Kraneveld, J.H.W. Leusen, L. Bont, B. Van''t Land, Maternal dietary fiber intake during lactation and human milk oligosaccharide fucosylation: a PRIMA birth cohort study, Mol. Nutr. Food Res. 69 (2025) e70165, https://doi.org/10.1002/mnfr.70165.
[44] A. Giorgetti, D. Paganini, S. Nyilima, R. Kottler, M. Frick, S. Karanja, T. Hennet, M. B. Zimmermann, The effects of 2′-fucosyllactose and lacto-N-neotetraose, galacto-oligosaccharides, and maternal human milk oligosaccharide profile on iron absorption in Kenyan infants, Am. J. Clin. Nutr. 117 (2023) 64–72, https://doi.org/10.1016/j.ajcnut.2022.10.005.
[45] M. Derrien, N. Mikulic, M.A. Uyoga, E. Chenoll, E. Climent, A. Howard-Varona, S. Nyilima, N.U. Stoffel, S. Karanja, R. Kottler, B. Stahl, M.B. Zimmermann, R. Bourdet-Sicard, Gut microbiome function and composition in infants from rural Kenya and association with human milk oligosaccharides, Gut Microbes 15 (2023) 2178793, https://doi.org/10.1080/19490976.2023.2178793.
[46] R. Burock, L. Chuzel, T. Kähne, U. Reichl, E. Rapp, R. Hennig, Raider of the lost N-glycans - localizing rare and frequently overlooked IgG N-glycans with sulfation or bisecting LacNAc, Front. Mol. Biosci. 12 (2025) 1593708, https://doi.org/10.3389/fmolb.2025.1593708.
[47] S.R.B.M. Eussen, M. Mank, R. Kottler, X.-K. Hoffmann, A. Behne, E. Rapp, B. Stahl, M.L. Mearin, B. Koletzko, Presence and levels of Galactosyllactoses and other oligosaccharides in human Milk and their variation during lactation and according to maternal phenotype, Nutrients 13 (2021), https://doi.org/10.3390/nu13072324.
[48] C. Wahl, D. Hirtz, L. Elling, Multiplexed capillary electrophoresis as analytical tool for fast optimization of multi-enzyme Cascade reactions - synthesis of nucleotide sugars: dedicated to prof. Dr. Vladimir Křen on the occasion of his 60th birthday, Biotechnol. J. 11 (2016) 1298–1308, https://doi.org/10.1002/biot.201600265.
[49] D. Laaf, P. Bojarová, H. Pelantová, V. Křen, L. Elling, Tailored multivalent neo-glycoproteins: synthesis, evaluation, and application of a library of Galectin-3-binding glycan ligands, Bioconjug. Chem. 28 (11) (2017) 2832–2840, https://doi.org/10.1021/acs.bioconjchem.7b00520.
[50] V. Heine, S. Boesveld, H. Pelantová, V. Křen, C. Trautwein, P. Strnad, L. Elling, Identifying efficient Clostridium difficile toxin a binders with a multivalent neo-glycoprotein glycan library, Bioconjug. Chem. 30 (9) (2019) 2373–2383, https://doi.org/10.1021/acs.bioconjchem.9b00486.
[51] A. Varki, R.D. Cummings, M. Aebi, N.H. Packer, P.H. Seeberger, J.D. Esko, P. Stanley, G. Hart, A. Darvill, T. Kinoshita, J.J. Prestegard, R.L. Schnaar, H. H. Freeze, J.D. Marth, C.R. Bertozzi, M.E. Etzler, M. Frank, J.F. Vliegenthart, T. Lütteke, S. Perez, E. Bolton, P. Rudd, J. Paulson, M. Kanehisa, P. Toukach, K. F. Aoki-Kinoshita, A. Dell, H. Narimatsu, W. York, N. Taniguchi, S. Kornfeld, Symbol nomenclature for graphical representations of Glycans, Glycobiology 25 (2015) 1323–1324, https://doi.org/10.1093/glycob/cwv091.
[52] Y. Kittel, L.P.B. Guerzoni, C. Itzin, D. Rommel, M. Mork, C. Bastard, B. Häßel, A. Omidinia-Anarkoli, S.P. Centeno, T. Haraszti, K. Kim, J. Guck, A.J.C. Kuehne, L. de Laporte, Varying the stiffness and diffusivity of rod-shaped microgels independently through their molecular building blocks, Angew. Chem. Int. Ed. 62 (2023) e202309779, https://doi.org/10.1002/anie.202309779.
[53] K. Pöstges, P. Palm, K.P. Hussnaetter, E. Filipová, H. Pelantová, L. Petrásková, P. Bojarová, V. Křen, L. Elling, Characterization of the human blood group glycosyltransferases GTA and GTB for the synthesis of blood group antigens, Adv. Synth. Catal. 368 (8) (2026) e70413, https://doi.org/10.1002/adsc.70413.
[54] Y. Bai, A.K. Agrahari, L. Zhang, H. Yu, X. Yang, Z. Zheng, W. Su, J. Fu, X. Chen, EASyMap-guided stepwise one-pot multienzyme (StOPMe) synthesis and multiplex assays identify functional Tetraose-Core-human Milk oligosaccharides, JACS Au 5 (2) (2025) 822–837, https://doi.org/10.1021/jacsau.4c01094.
[55] N. Lu, Y. Li, H. Xia, K. Zhong, C. Jia, J. Ye, X. Liu, C.-C. Liu, H. Cao, A redox-controlled substrate engineering strategy for site-specific enzymatic Fucosylation, Angew. Chem. Int. Ed. 61 (50) (2022) e202211032, https://doi.org/10.1002/anie.202211032.
[56] I.K. Sommerfeld, E.M. Dälken, L. Elling, A. Pich, Nitrilotriacetic acid functionalized microgels for efficient immobilization of Hyaluronan synthase, Macromol. Biosci. 24 (2024) e2400075, https://doi.org/10.1002/mabi.202400075.
[57] Y. Wu, Y. Sun, C. Pei, X. Peng, X. Liu, E.W. Qian, Y. Du, J.-J. Li, Automated chemoenzymatic modular synthesis of human milk oligosaccharides on a digital microfluidic platform, RSC Adv. 14 (2024) 17397–17405, https://doi.org/10.1039/D4RA01395F.
[58] S. Chakraborty, K. Minder, A.R. Prudden, G.-J. Boons, An automation platform for the Chemoenzymatic synthesis of complex sulfated and branched Glycans, J. Am. Chem. Soc. 148 (10) (2026) 11020–11032, https://doi.org/10.1021/jacs.5c22181.
[59] E. Makrydaki, R. Donini, A. Krueger, K. Royle, I.M. Ramirez, D.A. Kuntz, D.R. Rose, S.M. Haslam, K.M. Polizzi, C. Kontoravdi, Immobilized enzyme cascade for targeted glycosylation, Nat. Chem. Biol. 20 (2024) 732–741, https://doi.org/10.1038/s41589-023-01539-4.